Backscatter Relay Communications Powered by Wireless Energy Beamforming

Shimin Gong, *Member, IEEE*, Xiaoxia Huang, *Member, IEEE*, Jing Xu, *Member, IEEE*, Wei Liu, *Member, IEEE*, Ping Wang, *Senior Member, IEEE*, and Dusit Niyato, *Fellow, IEEE*

***Abstract*— The integration of wireless power transfer (WPT) with the low-power backscatter communications provides a promising way to sustain battery-less wireless networks. In this paper, we consider a backscatter communication network wirelessly powered by a power beacon station (PBS). Each backscatter radio uses the harvested energy to power its data transmissions, in which some other radios can help as the wireless relays with an aim to improve throughput performance by cooperative transmission. Under this setting, we formulate a throughput maximization problem to jointly optimize WPT and the relay strategy of the backscatter radios. An iterative algorithm with reduced complexity and communication overhead is proposed to decompose the original problem into two sub-problems distributed at the PBS and the backscatter receiver. Moreover, we take uncertain channel information into consideration and formulate robust counter-parts of the throughput maximization problem when either the backscatter or relay channel is subject to estimation errors. The difficulty of the robust counter-part lies in the coupling of the PBS' power allocation and relay strategy in matrix inequalities, which is addressed by alternating optimization with guaranteed convergence. Numerical results reveal that the cooperative relay strategy of the backscatter radios significantly improves the throughput performance.**

***Index Terms*— Backscatter communications, energy beamforming, wireless energy transfer, relay transmission.**

I. Introduction

With the explosive growth of wireless devices, it becomes impractical and costly to recharge or replace batteries for billions of wireless devices constituting the future Internet-of-Things (IoT). Wireless power transfer (WPT) is proposed as a promising technology to keep persistent connectivity of such IoT devices by allowing them to harvest energy from radio frequency (RF) signals [1]. The motivation for employing RF-based energy harvesting (EH) techniques are at least three-fold. Firstly, RF-based power transfer relies on far-field radiation. It supports better mobility of the charging devices and ensures scalability for device-to-device networks over a large geographical area. Secondly, the RF-based EH can reuse the same set of antennas for information communication. This supports simultaneous information and energy transfer, enabling the always-online system design for IoT applications. Moreover, the reuse of antennas supports highly integrated system design to minimize the size and improve the reliability of IoT devices, compared to the induction-based power transfer relaying on large coils at both the transceivers [2]. However, there is still a long way to widely deploy the RF-based WPT in wireless communications. One of the main challenges lies in the dilemma between the low efficiency in energy harvesting (EH) and the high power consumption in legacy transceivers. For example, the power consumption of Wi-Fi and Bluetooth devices ranges from several to a few hundred milliwatts, far beyond the EH rate from ambient RF signals [3].

To resolve this dilemma, one direct way is to increase the transmit power for WPT, e.g., the TX91501 Powercaster Transmitter with 3W power achieves the EH rate up to a hundred microwatts at the energy harvester within 5m range [3]. However, RF transmit power is subject to strict regulations by the authorities and may cause health concerns on RF radiation. A more plausible way lies in the development of extreme low power transceivers. The backscatter radios consume much less power in communications, namely, backscatter communications [4]–[7], by reflecting the incident RF signals instead of modulating information on self-generated carrier frequency. The information modulation is accomplished by adapting the load impedance and thus changing the antenna's reflection coefficient according to the baseband signals. As it does not require local oscillators to generate carrier signals and yet the power-consuming analog-to-digital/digital-to-analog convertors, the backscatter radios consume orders of magnitude less power than that of the conventional radios.

In a backscatter communication network, when WPT provides sufficient energy to power wireless communications, the backscatter radios are willingly serving as wireless relays for each other, with the aim to contribute a higher throughput

Manuscript received August 11, 2017; revised December 11, 2017; accepted February 17, 2018. Date of publication February 27, 2018; date of current version July 13, 2018. The work of Shimin Gong was supported in part by the National Natural Science Foundation of China (NSFC) under Grant 61601449, 61602462, Shenzhen Basic Research Program under Grant JCYJ20151117161854942, and Shenzhen Talent Peacock Plan Program under Grant KQTD2015071715073798. The work of Xiaoxia Huang was supported in part by NSFC-Guangdong Joint Program under Grant U1501255 and Guangdong Special Support Plan for Young Innovation Talents under Grant 2016TQ03X279. The work of Ping Wang was supported in part by Singapore MoE Tier 1 (RG 33/16). The work of Dusit Niyato was supported in part by Singapore MOE Tier 1 under Grant 2017-T1-002-007 RG122/17, MOE Tier 2 under Grant MOE2014-T2-2-015 ARC4/15, and NRF2015-NRF-ISF001-2277. The associate editor coordinating the review of this paper and approving it for publication was T. Q. Duong. *(Corresponding author: Xiaoxia Huang.)*

S. Gong is with the Shenzhen Institutes of Advanced Technology, Chinese Academy of Sciences, Shenzhen 518055, China (e-mail: sm.gong@siat.ac.cn).

X. Huang is with the College of Information Engineering, Shenzhen University, Shenzhen 518060, China (e-mail: xiaoxiah@gmail.com).

J. Xu and W. Liu are with the School of Electronic Information and Communications, Huazhong University of Science and Technology, Wuhan 430074, China (e-mail: xujing@hust.edu.cn; liuwei@hust.edu.cn).

P. Wang and D. Niyato are with the School of Computer Science and Engineering, Nanyang Technological University, Singapore 639798 (e-mail: wangping@ntu.edu.sg; dniyato@ntu.edu.sg).

Color versions of one or more of the figures in this paper are available online at http://ieeexplore.ieee.org.

Digital Object Identifier 10.1109/TCOMM.2018.2809613

via cooperative communications. Moreover, the backscatter radios' reflections of the incident signals mimic a spectrum-efficient full-duplex system with much simpler circuit implementation than that of conventional relays. Motivated by these observations, a backscatter relay protocol is proposed in this paper to assist the data transmission between two distant backscatter radios. WPT via beamforming design is also optimized to keep a balance between the backscatter communications in the source-relay and the relay-destination hops, which reveals a different tradeoff from that for conventional EH-enabled relay communications, e.g., [8]–[10].

A. Related Work

Backscatter communication is traditionally used in radio frequency identification (RFID) where a dedicated reader with high transmit power excites the communications with RFID tags in a short distance [4]. Ambient backscatter has been recently introduced to enable direct communications between two backscatter radios by reflecting the ambient RF signals from TV tower, cellular base stations, Wi-Fi and Bluetooth devices, e.g., [5]–[7], [11]–[13]. The performance of signal detection in ambient backscatter is characterized in [14]. Information theoretic study in [15] exploits the capacities of backscatter communication as well as ambient backscatter, revealing that ambient backscatter can achieve significant data rate over a short distance. A prototype of ambient backscatter developed in [5] achieves the rate of 1Kbps within 0.5m distance by exploiting the asymmetry in high-rate TV signals and low-rate backscatter transmissions. The BackFi backscatter system developed in [7] significantly improves the data rates up to 5Mbps within 1m and 1Mbps within 5m in the uplink communications with a full-duplex Wi-Fi access point. In [11], Kellogg *et al.* designed the passive Wi-Fi that allows backscatter radios to communicate with legacy Wi-Fi devices, with the data rate up to 11Mbps in the range of 10-30m and the power consumption less than 60μW. Leveraging the single tone of Bluetooth as the RF carrier signals, Iyer *et al.* [12] designed an backscatter system that synthesizes Wi-Fi signals with the data rate up to 11Mbps.

The backscatter radios' extreme low power consumption makes WPT a feasible solution to sustain backscatter communication networks. In one aspect, dedicated WPT from a power beacon station (PBS) can provide energy for backscatter radios. The harvested and stored energy can be used for data preprocessing and access control of multiple radios. In another aspect, the power beacon also provides the carrier signal for backscatter communications. Hence, the design of WPT strategy has to account for the tradeoff at different backscatter radios. Arnitz and Reynolds [16] and Yang *et al.* [17] optimized the energy beamforming from a multi-antenna PBS to multiple backscatter radios without or with limited channel estimations at the destined receivers. In [18], Han and Huang proposed a network architecture for wireless powered backscatter communications and analyzed the network coverage and capacity by a stochastic geometric approach. In [19], Hoang *et al.* adopted backscatter communications into the wireless powered cognitive radio networks, and showed significant performance improvement for the secondary transmitters. Data scheduling and admission control in a sensor network have been studied in [20] to ensure efficient data collection via backscatter communications from multiple wireless sensors with prioritized packets.

Relay communication has been studied extensively for conventional radios with EH capability by considering a single relay in [8], multiple relays in [21], and a multi-access relay model in [22], etc. The relays' transmit power and data rate are constrained by the amount of harvested energy, and thus it is preferable to maximize the energy transfer to the relays. The backscatter radios transmit information by modulating and directly reflecting the incident signals. The strength of incident signals, rather than the amount of energy harvested by the backscatter relays, dictates the data rate of backscatter communications. Thus, it will be more preferable to increase the strength of incident signals, or the transmit power at the source node. This implies that the existing power-splitting and time-switching based relay strategies are inefficient for backscatter radios, which motivates our study in this work.

B. Our Contributions

In this work, we consider a backscatter communication network wirelessly powered by a multi-antenna PBS, which is dedicated to beamforming energy according to the radios' channel conditions and energy status. Similar to a bistatic backscatter configuration [23], the PBS also serves as the carrier emitter for backscatter communications. To avoid control overhead in competing channel access, we consider a time division multiple access (TDMA) scheme, i.e., each backscatter radio talks to its receiver in a dedicated time slot via backscatter communication and harvests RF energy in other time slots. This model can be envisioned as a wireless sensor network deployed in manufactories or buildings where the sensors in different locations monitor malfunctionings or structural faults, e.g., [21]. The sensors are required to report sensing results to a common control node (e.g., data fusion center) regularly. Due to a large number of sensors and the complex monitoring environment, the battery-less sensors will be more preferable and can be designed to work via backscatter communications, with the assistant of a few wall-amounted on-grid power emitters.

We focus on the case when the direct path from the backscatter transmitter to the receiver is weak due to a long distance between the transceiver. To improve the data rate, we propose a two-hop PBS-assisted backscatter relay protocol that relies on the PBS to enhance signal reception at the receiver. Specifically, we divide each time slot into two sub-slots. In the first slot, the source node sends information to the PBS via backscatter communication. In the second hop, the PBS forwards the decoded information to the receiver, meanwhile the relays backscatter the PBS' signals to enhance the signal strength at the receiver. Compared to the harvest-store-use (HSU) protocol for conventional EH-enabled relays [8], the proposed backscatter relay protocol admits several advantages. Firstly, there is no dedicated channel time or signal power to charge the relays, making it more

spectrum- and energy-efficient. Secondly, in the first hop, by a joint design of the carrier signals emitted by the PBS and the load modulation scheme at the source note, we can achieve a few megabyte data rate via backscatter communication, with the power consumption significantly less than that of a typical Wi-Fi system [11]. Moreover, the set of relays in the second hop form a distributed MIMO backscatter system, which can improve the transmission range and capacity [24]. Measurement results in [25] reveal that the signal detection performance can be enhanced significantly by the assistance of backscattered signals from multiple antennas.

Despite of its advantages, the implementation of backscatter relay protocol also faces several challenges. As the channel conditions vary at different radios, the first challenge is to select an optimal set of backscatter radios to join the relay transmission. The PBS' energy beamforming not only provides the carrier signal for backscatter communication in the first hop, but also powers the relays in the second hop. The carrier signal can be enhanced by steering the beamformer towards the source node, which can improve the data rate in the first hop but on the other hand impair the power transfer to the relays. Hence, the relay selection is complicated by the coupling between achieving higher data rate in the first hop and powering more relays in the second hop. Given the set of relays, another challenge lies in the joint design of the relays' reflection coefficients to enhance the signal reception, especially when the channel estimations are subject to errors. We aim to address above challenges in this paper and our main contributions are summarized as follows:

1) *Two-hop PBS-Assisted Backscatter Relay Scheme:* To the best of our knowledge, we are the first to propose backscatter radios as the wireless relays for a distant transceiver pair. In the proposed relay scheme, the PBS beamforms energy or carrier signals to the source node and decodes the backscattered information in the first hop. Then, in the second hop, the PBS beamforms the decoded information to the relays and meanwhile the backscatter relays reflect the PBS' signal to enhance signal reception at the targeted receiver. Without information decoding at the relays, this protocol minimizes the relays' energy consumption and better motivates them to join the cooperative transmission.
2) *Joint Optimization of WPT and Relay Strategy:* We formulate a throughput maximization problem that jointly optimizes the relay strategy and the PBS' beamforming in two hops. Though the problem is non-convex, we present a semi-definite relaxation that can be solved optimally in a centralized manner. To further reduce its complexity, we propose an iterative algorithm that decomposes the original problem into two subproblems distributed at the PBS and the backscatter receiver. We also design an adaptive relay strategy that updates the set of relays iteratively to achieve a better throughput.
3) *Enhance Robustness Against Channel Uncertainty:* We propose a robust counter-part of the throughput maximization problem when the errors in channel estimation are uncertain but bounded in convex sets. The difficulty of the robust counter-part lies in the coupling of the PBS' power allocation and relay strategy in matrix inequalities. With fixed power allocation (or relay strategy), the robust relay strategy (or power allocation) can be easily found by solving a semi-definite program (SDP). Hence, we maximize the robust performance by alternating optimization that solves two SDPs iteratively with guaranteed convergence.

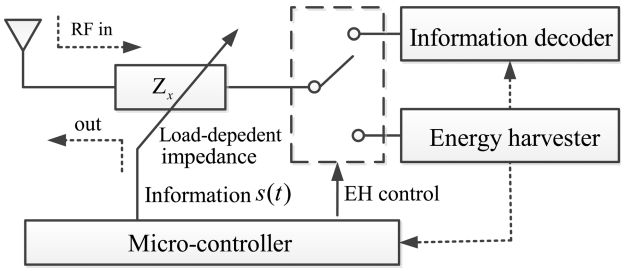

Fig. 1. Wireless powered radio for backscatter communication.

The remainder of this paper is organized as follows. In Section II, we introduce the system model and propose the backscatter relay model. In Section III, we address a throughput maximization problem by jointly optimizing the PBS' energy beamforming and the relay strategies. In Section IV, we study the robust relay strategies to enhance the throughput performance with uncertain channel information. Simulations and conclusions are given in Sections V and VI, respectively.

Notations: We use $\mathbb{C}$ to denote the set of complex numbers and $\mathrm{Re}(\cdot)$ to denote the real part of a complex number. $|\cdot|$, $||\cdot||$ and $||\cdot||_F$ denote the absolute value, Euclidean norm, and Frobenius norm, respectively. $\mathbb{P}(\cdot)$ stands for the probability of an event and $\mathbb{E}[\cdot]$ denotes the expectation operation. We have $\mathbf{Tr}(\cdot)$, $(\cdot)^T$ and $(\cdot)^H$ to take the trace, transpose, and conjugate transpose of a matrix, respectively. The operator $\otimes$ denotes Kronecker product and $\mathrm{vec}(\cdot)$ reshapes a matrix into a vector by cascading all column vectors.

II. System Model

We envision a device-to-device (D2D) network under the coverage of a multi-antenna PBS, which beamforms RF signals to power the D2D user equipments (DUEs), all equipped with single antenna. The set of DUE transceiver pairs is denoted by $\mathcal{N} = \{1, 2, \ldots, N\}$. The PBS also serves as a coordinator scheduling the DUEs' data transmissions. In particular, each DUE $n \in \mathcal{N}$ is allocated a fixed time slot with unit length for its data transmission, and can harvest RF energy in the time slot allocated to any other DUE $m \in \mathcal{N}$, $m \neq n$. Each DUE transmits information via backscatter communication by modulating and reflecting the ambient RF signals. This is achieved by changing the load impendence according to the intended information bits $s(t)$, that is, load modulation. For signal reception, the DUE tunes the load impedance Z_x to match the antenna impedance and thus ensure the maximum efficiency in signal reception. The structure of DUEs' radio is illustrated in Fig. 1. The most common circuit implementation of load modulation is by switching between different states of impedance. Given the varying load impedance, the reflected

RF signals will have different power levels, which can be used to retrieve the information $s(t)$ at the receiver.

A. Direct Backscatter

For any DUE pair $n \in \mathcal{N}$, the channels from the PBS to the n-th DUE transmitter (DTx-n) and the n-th DUE receiver (DRx-n) are denoted by $\mathbf{h}_n \in \mathbb{C}^M$ and $\mathbf{f}_n \in \mathbb{C}^M$, respectively, where M denotes the number of antennas at the PBS. Each channel is considered as frequency-flat block fading [26], i.e., the channel coefficients are constant in one data frame and may change frame by frame. We focus on data transmissions of the transceiver pair DTx/DRx-0 to derive the signal models. Let $\hat{\mathbf{w}}$ denote normalized beamforming vector at the PBS. The signal emitted by the PBS is given as

$$\mathbf{w}(t) = \sqrt{p_e}\hat{\mathbf{w}}u(t), \tag{1}$$

where p_e denotes the PBS' beamforming power and $u(t)$ is a known sequence with unit power. For example, $u(t)$ can be a single-tone sinusoidal signal to enable high speed backscatter communications, e.g., [11]. Then, the received signal at DTx-0 can be represented by $b(t) = \mathbf{h}_0^H \mathbf{w}(t) + \sigma_t$, where σ_t denotes the complex Gaussian noise at the antenna. Meanwhile, DTx-0 modulates its information $s(t)$ on the ambient signal $b(t)$ by controlling its reflection coefficient $\Gamma_0(t) = \Gamma_0\ s(t)$, where $\Gamma_0 \in \mathbb{C}$ is an antenna-specific constant coefficient. Then, the signal received by the DRx-0 is given by

$$y(t) = g_0\Gamma_0\mathbf{h}_0^H\mathbf{w}(t)s(t) + \mathbf{f}_0^H\mathbf{w}(t) + g_0\Gamma_0\sigma_t s(t) + v_r, \tag{2}$$

where $g_0 \in \mathbb{C}$ represents the *backscatter channel* from the DTx-0 to the DRx-0 and $v_r \backsim \mathcal{CN}(0,1)$ denotes the complex Gaussian noise at baseband, normalized to zero mean and unit variance. The first term in $y(t)$ contains the information $s(t)$ dedicated to the DRx-0. The second term $\mathbf{f}_0^H\mathbf{w}(t)$ is due to direct energy beamforming from the PBS to the DRx-0. The third term $g_0\Gamma_0\sigma_t s(t)$ contains the antenna noise σ_t forwarded to the DRx-0. In a practical case, both of the antenna and baseband noises have comparable power levels [27]. After the attenuation by the channel g_0, the power of the third term will be much smaller than that of v_r and hence we omit it in our subsequent derivations.

Assuming known signal $\mathbf{w}(t)$ and channel $\mathbf{f}_0$, by self-interference cancelation, the second part can be subtracted from the received signal and will not introduce interference to the receiver [7]. Without loss of generality, assuming $\mathbb{E}[|s(t)|^2] = 1$, the data rate of backscatter communication from the DTx-0 to the DRx-0 can be represented as follows:

$$r_D = \log\Big(1 + |\Gamma_0|^2|g_0|^2\mathbb{E}[|\mathbf{h}_0^H\mathbf{w}(t)|^2]\Big). \tag{3}$$

In fact, the exact data rate of backscatter communications is difficult to characterize, due to non-Gaussian distribution of the combined noise terms in (2). Assuming that the power of backscattered noise is much smaller than that of the baseband noise, we can use (3) as an approximation of the data rate.

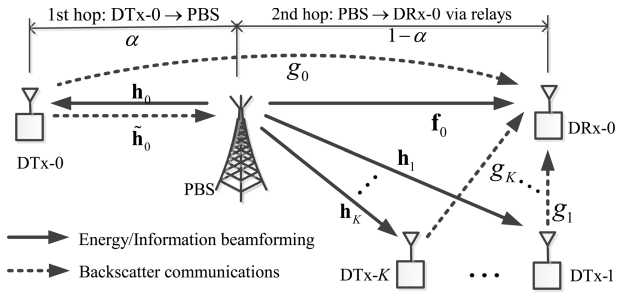

Fig. 2. Two-hop backscatter relay communication.

B. Relay Backscatter

Backscatter communication requires significantly (typically orders of magnitude) less power than that of the conventional radios modulating information on self-generated carrier frequency signals. When the PBS' energy beamforming easily fulfills the backscatter radios' power demands, the DUEs are willing to act as wireless relays for each other, aiming to achieve a higher throughput via cooperative transmissions. *Backscatter relay communication*, leveraging the PBS, can be implemented in a time-slotted protocol. In particular, we divide the unit time slot into two sub-slots by a slot splitting parameter α, and assume that the transmission of the DTx/DRx-0 is assisted by a set of relays, denoted by $\mathcal{R} \triangleq \{1, 2, \ldots, K\} \subset \mathcal{N}$. An illustration of the system model is shown in Fig. 2. In the first sub-slot, the on-grid PBS serves as a carrier emitter for DTx-0 to modulate its information $s(t)$ in the air and mimic Wi-Fi data transmission via backscatter communication, similar to the passive Wi-Fi system developed in [11]. In this manner, the data rate can reach up to 11Mbps while the power consumption is less than 60μW.

After information decoding at the PBS, it beamforms $s(t)$ to the DRx-0 in the second sub-slot, meanwhile the relays backscatter the PBS' signals to enhance signal reception at the DRx-0. Compared to conventional relays, the backscatter relays can be more efficient in both energy and channel usage, as they mimic full-duplex relay communications by a much simpler circuit implementation. Moreover, the relays do not require information decoding before backscattering, and thus minimize the energy consumption for relay transmissions, which can better motivate the relays to join the cooperative transmissions. What worth mentioning is that, in the second hop, the backscatter relays reflect all incident signals to enhance signal strength at the DRx-0, without modulating any information on the reflected signals. To this end, the relays can set fixed reflection coefficients according to individuals' channel conditions. The received signals at the DRx-0 is a mixture of the signals from the PBS' active transmission and the reflections of the relays. By controlling the relays' reflection coefficients, we can achieve constructive multi-path effect at the DRx-0 and thus improve the data rate in the second hop. However, the online optimization and tuning of the reflection coefficients are difficult in system implementation. Practically we can pre-design a number of load impedances to construct a finite codebook of reflection coefficients. Each load impedance can be chosen from the codebook by a multi-throw switch to best match the required reflection coefficient [28].

Let $\tilde{\mathbf{h}}_0$ denote the uplink channel from the DTx-0 to the PBS. After self-interference cancelation at the PBS, the received signal is given by

$$y_p = \Gamma_0 \mathbf{w}_p^H \tilde{\mathbf{h}}_0 \mathbf{h}_0^H \mathbf{w}(t) s(t) + v_p,$$

where $v_p \sim \mathcal{CN}(0, 1)$ is the received noise at the PBS and $\mathbf{w}_p$ is the combining ratio. Without loss of generality, we assume that Γ_0 is one and omitted in the following derivation. By maximum ratio combining, we have $\mathbf{w}_p^* = \tilde{\mathbf{h}}_0 / ||\tilde{\mathbf{h}}_0||$ and the throughput in the first hop is given by

$$r_1 = \alpha \log \left(1 + p_e ||\tilde{\mathbf{h}}_0||^2 |\mathbf{h}_0^H \hat{\mathbf{w}}|^2\right). \tag{4}$$

The first sub-slot is also used for powering the relays via WPT. Given a power demand (or sensitivity) p_b at the backscatter relays, the power budget constraints are given by

$$\eta \alpha p_e |\mathbf{h}_k^H \hat{\mathbf{w}}|^2 \geq (1 - \alpha) p_b, \quad \forall k \in \mathcal{R}, \tag{5}$$

where η denotes the energy conversion coefficient. The sensitivity p_b is mainly determined by the architecture of RF front end and the fabrication process [29], which can be lower than -40dBm. Note that p_b can vary at the relays due to different sensitivities in the antenna. This variation will not affect our analysis as follows and thus, for simplicity, we assume that p_b is the same for all relays. In the power budget constraint (5), we actually assume a linear EH model with constant power conversion efficiency η, i.e., the total harvested energy is linearly dependent on the strength of RF signals at the receiving antenna. A more practical nonlinear EH model has been presented in [30], in which η is measured to be dependent on the strength of RF signals. Let $\Phi_k(\hat{\mathbf{w}})$ denote the energy harvested from the PBS. The nonlinear dependency on $\hat{\mathbf{w}}$ can be captured by a logistic function as follows:

$$\Phi_k(\hat{\mathbf{w}}) = (1 - \Omega_k)^{-1} \left(\Psi_k(\hat{\mathbf{w}}) - \Omega_k M_k\right), \tag{6}$$

where $\Psi_k \triangleq M_k \left(1 + e^{-a_k \left(p_e |\mathbf{h}_k^H \hat{\mathbf{w}}|^2 - b_k\right)}\right)^{-1}$. The parameters M_k and (a_k, b_k) can be estimated via measurement data. The constant Ω_k ensures $\Phi_k(\hat{\mathbf{w}}) = 0$ when $p_e = 0$. However, we can show that a nonlinear model will not fundamentally change our problem formulation. In particular, replacing $\eta p_e |\mathbf{h}_k^H \hat{\mathbf{w}}|^2$ by $\Phi_k(\hat{\mathbf{w}})$ and after some manipulations, we can reformulate the power budget constraint in (5) as follows:

$$p_e |\mathbf{h}_k^H \hat{\mathbf{w}}|^2 \geq b_k + \frac{1}{a_k} \log \left(\frac{(1 - \Omega_k) p_b' + M_k \Omega_k}{(1 - \Omega_k)(M_k - p_b')}\right). \tag{7}$$

Obviously, the new constraint (7) has the same form as that in (5), which implies that our subsequent analysis and algorithm design also apply to the nonlinear EH model (6).

Assuming error free information decoding at the PBS, in the second hop, the PBS beamforms the signal $\mathbf{v}(t) = \sqrt{p_s} \hat{\mathbf{v}} s(t)$ to the DRx-0, where $\hat{\mathbf{v}}$ is the *normalized* beamforming vector and p_s denotes the PBS' transmit power. The feasible set of power allocation (p_e, p_s) in two hops is defined as follows:

$$\mathcal{P}(\alpha) \triangleq \left\{ (p_e, p_s) \,\middle|\, \begin{array}{c} \alpha p_e + (1 - \alpha) p_s \leq e_{\max}, \\ p_e, \quad p_s \in (0, p_{\max}) \end{array} \right\}, \tag{8}$$

where $e_{\max}$ denotes the PBS' energy limit in one time slot and $p_{\max}$ is the maximum transmit power due to hardware constraint. Given the reflection coefficient Γ_k of each backscatter relay $k \in \mathcal{R}$, the received signal at DRx-0 is given by

$$y_d = \sum_{k \in \mathcal{R}} g_k \Gamma_k \sqrt{p_s} \mathbf{h}_k^H \hat{\mathbf{v}} s(t) + \sqrt{p_s} \mathbf{f}_0^H \hat{\mathbf{v}} s(t) + v_d, \tag{9}$$

where $v_d \sim \mathcal{CN}(0, 1)$ is the noise at the receiver and g_k denotes the *backscatter channel* from DTx-k to DRx-0. The first term in y_d denotes the aggregated signals reflected by the relays and the second term corresponds to a direct path from the PBS to DRx-0. Define $\mathbf{x} = [\Gamma_1, \Gamma_2, \ldots, \Gamma_K]^T$ and $\mathbf{H} = [\mathbf{h}_1, \mathbf{h}_2, \ldots, \mathbf{h}_K]$, then the SNR of the DRx-0 is given by $\gamma_d = p_s \left|(\mathbf{H} \mathrm{D}(\mathbf{g}) \mathbf{x} + \mathbf{f}_0)^H \hat{\mathbf{v}}\right|^2$, where $\mathrm{D}(\mathbf{g})$ denotes a diagonal matrix with the diagonal element specified by the channel vector $\mathbf{g} = [g_1, g_2, \ldots, g_K]^T$. Hence, the throughput in the second hop is given as follows:

$$r_2 = (1 - \alpha) \log \left(1 + p_s |(\mathbf{B}\mathbf{x} + \mathbf{f}_0)^H \hat{\mathbf{v}}|^2\right), \tag{10}$$

where $\mathbf{B} \triangleq \mathbf{H} \mathrm{D}(\mathbf{g}) = [g_1 \mathbf{h}_1, g_2 \mathbf{h}_2, \ldots, g_K \mathbf{h}_K]$ and $\mathbf{b}_k \triangleq g_k \mathbf{h}_k$ can be viewed as the k-th *relay channel* from the PBS to DRx-0 via DTx-k.

III. Throughput Maximization in Backscatter Relay Communication

To maximize the *effective throughput* $r \triangleq \min(r_1, r_2)$, we first require an optimal slot splitting parameter α, which relates the throughput of backscatter communication in the first hop and the number of cooperative backscatter relays in the second hop. A larger α implies that more relays can harvest sufficient energy to remain active, however, with the price of reduced transmission time in the second sub-slot. To analyze the performance tradeoff, we formulate a throughput maximization problem by jointly optimizing the slot splitting parameter α, the relays' reflection coefficients $\mathbf{x}$, the PBS' power allocation (p_e, p_s) and beamforming strategy $(\hat{\mathbf{w}}, \hat{\mathbf{v}})$:

$$\max_{\alpha, p_e, p_s, \hat{\mathbf{w}}, \hat{\mathbf{v}}, \mathbf{x}} \ \min \left(r_1(\alpha, \hat{\mathbf{w}}), r_2(\alpha, \hat{\mathbf{v}}, \mathbf{x})\right) \tag{11a}$$

$$s.t. \ (p_e, p_s) \in \mathcal{P}(\alpha) \text{ and } (5), \tag{11b}$$

$$||\hat{\mathbf{w}}|| \leq 1, \quad ||\hat{\mathbf{v}}|| \leq 1, \ |\Gamma_k| \leq 1, \ \forall k \in \mathcal{R}. \tag{11c}$$

The expressions of data rates r_1 and r_2 in the objective are given in (4) and (10), respectively. Relay backscatter is preferred if it achieves higher throughput than that of the direct backscatter. To analyze the conditions under which relay backscatter is preferred, it suffices to study a lower bound of problem (11) and compare it to the throughput r_D achieved by direct backscatter. In the proposed relay model, the backscatter relays enhance the PBS' signal at the DRx-0. Hence, the lower bound of (11) can be obtained when there is no relay assisting the PBS' signal transmission. In this case, we can simply maximize the throughput in the first and second sub-slots, respectively. Given the parameter α, the maximum throughput in the first sub-slot is achieved by aligning the energy beamformer to the channel $\mathbf{h}_0$, i.e., $\hat{\mathbf{w}} = \hat{\mathbf{h}}_0 \triangleq \mathbf{h}_0 / ||\mathbf{h}_0||$, and then we have $r_1 = \alpha \log \left(1 + p_e ||\mathbf{h}_0||^4\right)$. Here we assume $\tilde{\mathbf{h}}_0 = \mathbf{h}_0$ due to channel reciprocity. Similarly, the maximum throughput

in the second sub-slot can be achieved by setting $\hat{\mathbf{v}} = \mathbf{f}_0/||\mathbf{f}_0||$, i.e., $r_2 = (1-\alpha)\log\left(1 + p_s||\mathbf{f}_0||^2\right)$. Note that r_1 is increasing while r_2 is decreasing in α. The optimal α^* can be obtained by a bisection method and achieved when $r_1 = r_2 = r_R$. Hence, relay backscatter is preferred if $r_R \geq r_D$, which implies

$$p_e|\Gamma_0|^2|g_0|^2||\mathbf{h}_0||^2 \leq \left(1 + p_s||\mathbf{h}_0||^4\right)^{\alpha^*} - 1. \tag{12}$$

This result verifies that relay backscatter can improve the data rate when the direct path g_0 is weak. The inequality (12) helps determine a preferable region for relay backscatter. The channel estimation and the dissemination of PBS' choice can be performed in the beginning of each time slot.

In the sequel, we consider a general case in which relay backscatter is motivated, and we aim to find the optimal relay strategy that maximizes the overall throughput. Our numerical results in Section V show that the effective throughput has a concave structure in the parameter α. This implies that we can apply a gradient-based method to determine the optimal α^* efficiently. In particular, we can first use one-dimension search over (0, 1) with a relatively large grid size to determine a preferred region of α, and then apply the gradient-based method to iterate until α^*. For conciseness, we fix α in this paper and focus on the solution $\{p_e, p_s, \hat{\mathbf{w}}, \hat{\mathbf{v}}, \mathbf{x}\}$ to (11).

A. Semi-Definite Relaxation (SDR) to (11)

Problem (11) is challenging firstly due to the coupling of the PBS' power allocation in two hops. More power in the first sub-slot implies a higher data rate in the first hop and more cooperative relays for the second hop, which implies that an optimal power allocation is required to balance the data rate in both hops. Moreover, the PBS' energy beamforming in the first hop also needs to strike a balance between the uplink data rate from the DTx-0 to the PBS and the downlink energy transfer from the PBS to the backscatter relays. Intuitively, if the relays can harvest sufficient energy from ambient RF signals, e.g., in the case of small p_b, it is optimal to align $\hat{\mathbf{w}}$ with the channel $\mathbf{h}_0$ to maximize the data rate in the first hop. If EH is insufficient to power the relays, i.e., in the case of relatively large p_b, the PBS needs to adjust its beamformer to increase the rate of WPT towards the relays, with a cost of decrease in the data rate of the first hop. When channel conditions become worse off and p_b is beyond the relays' EH capabilities, relay backscatter is not preferred and it is better for the PBS to steer the beamformer back to the DTx-0.

Note that $\hat{\mathbf{v}}$ and $\mathbf{x}$ only present in the rate constraint $r_2(\alpha, \hat{\mathbf{v}}, \mathbf{x}) \geq r$. The optimal $\hat{\mathbf{v}}^*$ maximizing r_2 is aligned to the equivalent channel $\mathbf{f}_\mathbf{x} \triangleq \mathbf{B}\mathbf{x} + \mathbf{f}_0$, i.e., $\hat{\mathbf{v}}^* = \hat{\mathbf{f}}_\mathbf{x} \triangleq \mathbf{f}_\mathbf{x}/||\mathbf{f}_\mathbf{x}||$. Hence, given the fixed α and the PBS' power allocation (p_e, p_s), the data rate r_2 only relates to $||\mathbf{f}_\mathbf{x}||$ and depends on the relays' reflection coefficients $\mathbf{x}$. Unfortunately, the optimization of relays' reflection coefficients falls into a non-convex quadratic problem [31]. To proceed, we introduce two positive semi-definite (PSD) matrices such that $\mathbf{W} = \hat{\mathbf{w}}\hat{\mathbf{w}}^H$ and $\mathbf{X} = \mathbf{x}\mathbf{x}^H$. By dropping the rank-one constraints on $\mathbf{W}$ and $\mathbf{X}$, the SDR representation of (11) is given as follows:

$$\max_{r, p_e, p_s, \mathbf{W}, \mathbf{X}, \mathbf{x}} \quad r \tag{13a}$$

$$s.t.\ \ p_e\mathbf{h}_0^H\mathbf{W}\mathbf{h}_0 \geq \bar{\gamma}_1(\alpha, r), \tag{13b}$$

$$p_s||\mathbf{B}\mathbf{x} + \mathbf{f}_0||^2 \geq \bar{\gamma}_2(\alpha, r), \tag{13c}$$

$$p_e\mathbf{h}_k^H\mathbf{W}\mathbf{h}_k \geq \bar{p}_b, \quad \forall k \in \mathcal{R}, \tag{13d}$$

$$(p_e, p_s) \in \mathcal{P}(\alpha) \text{ and } (\mathbf{W}, \mathbf{X}) \in \mathcal{M}, \tag{13e}$$

where we define $\mathcal{M} \triangleq \{\mathbf{W} \succeq \mathbf{0} | \mathbf{Tr}(\mathbf{W}) \leq 1\} \times \{\mathbf{X} \succeq \mathbf{x}\mathbf{x}^H | \mathbf{X}_{kk} \leq 1,\ \forall k \in \mathcal{R}\}$. The power threshold $\bar{p}_b$ is given by $(1-\alpha)p_b/(\eta\alpha)$. Given the throughput r and parameter α, the target rates in two hops are given by $\bar{\gamma}_1(\alpha, r) = ||\tilde{\mathbf{h}}_0||^{-2}\left(e^{r/\alpha} - 1\right)$ and $\bar{\gamma}_2(\alpha, r) = e^{r/(1-\alpha)} - 1$, respectively.

To maximize r, we can first check the feasibility of (13) with some fixed r, and then update r accordingly in a bisection method. Though the transmit power p_e is coupled with $\mathbf{W}$ in a non-convex form as in (13b) and (13d), we can easily transform them into linear matrix inequalities. Besides, the quadratic term $||\mathbf{B}\mathbf{x} + \mathbf{f}_0||^2$ in (13c) can be rewritten as $L(\mathbf{X}, \mathbf{x}) \triangleq \mathbf{Tr}(\mathbf{B}\mathbf{X}\mathbf{B}^H) + 2\mathrm{Re}(\mathbf{f}^H\mathbf{B}\mathbf{x}) + \mathbf{f}_0^H\mathbf{f}_0$, which is linear in $\mathbf{X}$ and $\mathbf{x}$. Hence, the same transformation for (13b) and (13d) also applies to (13c). In particular, the convex reformulations of (13b) and (13c) are given by

$$\begin{bmatrix} p_e & \bar{\gamma}_1^{1/2} \\ \bar{\gamma}_1^{1/2} & \mathbf{h}_0^H\mathbf{W}\mathbf{h}_0 \end{bmatrix} \succeq 0 \text{ and } \begin{bmatrix} p_s & \bar{\gamma}_2^{1/2} \\ \bar{\gamma}_2^{1/2} & L(\mathbf{X}, \mathbf{x}) \end{bmatrix} \succeq 0,$$

respectively. With fixed α and r in the bisection iteration, the constraints (13b)-(13e) are actually all linear inequalities and the feasibility check of (13) becomes a semi-definite program (SDP) efficiently tractable by interior-point algorithms with the computational complexity $O\left(K^{2.5}M^4 + K^{6.5}\right)$, where K and M denote the number of relays and the number of the PBS' antennas, respectively [32]. The centralized solution not only consumes considerable computational resource at the PBS, but also requires the collection of complete channel information $\{\mathbf{h}_0, \mathbf{h}_1, \ldots, \mathbf{h}_K, \mathbf{f}, \mathbf{g}\}$ beforehand. This can be achieved by channel estimation at different devices and collected by the PBS. In particular, the PBS can estimate the channel $\mathbf{h}_i$ sequentially by overhearing a pilot signal from each DTx-i, $i \in \{0, 1, \ldots, K\}$. The estimate of $\{\mathbf{f}_0, \mathbf{g}\}$ can be performed similarly at the DRx-0 and returned back to the PBS.

B. Decomposed Solution to (11)

To reduce computational complexity and communication overhead, we aim to break the tie between the two hops, and correspondingly decompose problem (13) into two sub-problems with smaller size based on local channel information. Specifically, we note that (13c) is coupled with (13b) and (13d) through the PBS' power allocation in (13e). The optimization of $\mathbf{W}$ only depends on the feasibility of (13b) and (13d), while the optimization of $\mathbf{X}$ and $\mathbf{x}$ relates to (13c). This observation motivates us to first maximize the norm $||\mathbf{B}\mathbf{x} + \mathbf{f}_0||$ in (13c) and then replace (13c) by a linear constraint in p_s:

$$p_s||\mathbf{B}\mathbf{x}^* + \mathbf{f}_0||^2 \geq \bar{r}_2(\alpha, r), \tag{14}$$

where $\mathbf{x}^*$ denotes the maximizer of $||\mathbf{B}\mathbf{x}+\mathbf{f}_0||^2$. The other subproblem is to check feasibility of (13b) subject to the power budget constraint (13d). The result of feasibility check then drives the update of data rate r in a bisection method. We list the decomposed solution procedure in Algorithm 1.

Algorithm 1 Energy Beamforming and Relay Backscatter

Input: The relay set $\mathcal{R}$, the parameters p_b and α

Output: The beamformer $\mathbf{w}$ and reflection coefficient $\mathbf{x}$

1: Initialize r_{min}, r_{max}, and channel information $(\mathbf{h}_k, \mathbf{f}_0, g_k)$

2: **loop**

3: $r \leftarrow (r_{max} + r_{min})/2$

4: Maximize $||\mathbf{B}\mathbf{x} + \mathbf{f}_0||^2$ in the second hop:

$$\max_{\mathbf{x}} \quad \{||\mathbf{B}\mathbf{x} + \mathbf{f}_0||^2 : ||x_k|| \le 1, \quad \forall k \in \mathcal{R}\}. \tag{15}$$

5: Maximize data rate in the first hop:

$$\max_{\mathrm{Tr}(\mathbf{W}) \le p_{\max}} \quad \mathbf{h}_0^H \mathbf{W} \mathbf{h}_0 \tag{16a}$$

$$s.t.\ \mathbf{h}_k^H \mathbf{W} \mathbf{h}_k \ge \bar{p}_b, \quad \forall k \in \mathcal{R} \tag{16b}$$

$$p_s ||\mathbf{B}\mathbf{x}^* + \mathbf{f}_0||^2 \ge \bar{r}_2(\alpha, r) \tag{16c}$$

$$\alpha \mathrm{Tr}(\mathbf{W}) + p_s(1-\alpha) \le e_{\max}. \tag{16d}$$

6: Extract rank-one $\hat{\mathbf{w}}$ from $\mathbf{W}$ by eigen-decomposition

7: **if** $\mathbf{h}_0^H \mathbf{W} \mathbf{h}_0 < \bar{\gamma}_1$, $r_{\max} \leftarrow r$ **else** $r_{\min} \leftarrow r$ **end if**

8: **loop until** r converges to its maximum

9: The PBS distributes the relay strategy to DUEs

The maximization of $||\mathbf{B}\mathbf{x} + \mathbf{f}_0||^2$ in line 4 of Algorithm 1 is actually NP-hard [31]. Though SDR provides a convex reformulation of $||\mathbf{B}\mathbf{x} + \mathbf{f}_0||^2$ in problem (15), it admits a performance gap when the rank-dropped optimal solution $\mathbf{X}^*$ is actually of high rank. In this case, we face the practical challenge to recover a rank-one approximate solution $\mathbf{x}^*$, which is often problem-specific and heuristic. The authors in [33] and [34] overcome such difficulty by designing an successive approximation method that rewrites the non-convex quadratic terms by their affine approximations. In this paper, we aim to improve the performance of SDR solution by designing additional search algorithm to update the SDR solution. A similar idea has been presented in [35]. By introducing auxiliary variables $\{\mathbf{z}_k\}_{k\in\mathcal{R}}$, we can rewrite (15) as follows:

$$\min_{\mathbf{x}, \mathbf{z}_k} \ f(\mathbf{x}) \triangleq -\mathbf{x}^H \mathbf{B}\mathbf{B}^H \mathbf{x} - 2\mathrm{Re}(\mathbf{f}_0^H \mathbf{B}\mathbf{x}) \tag{17a}$$

$$s.t.\ |\mathbf{e}_k^H \mathbf{z}_k| \le 1 \text{ and } \mathbf{z}_k = \mathbf{x}, \quad k \in \mathcal{R}, \tag{17b}$$

where $\mathbf{e}_k$ denotes the unit vector with "1" at the k-th entry. As revealed in the sequel, this reformulation allows us to decouple the quadratic constraints on $\mathbf{x}$ and solve multiple quadratic problems sequentially with guaranteed rank-one solutions.

To proceed, we can place the equality constraint in (17b) into the objective by introducing dual variable $\mathbf{y}_k$ and a penalty term, resulting in the augmented Lagrangian as follows:

$$\begin{aligned}\Gamma(\mathbf{x}, \mathbf{z}_k, \mathbf{u}_k) &= f(\mathbf{x}) + \sum_{k\in\mathcal{R}} \left(\mathbf{y}_k^T(\mathbf{z}_k - \mathbf{x}) + \rho||\mathbf{z}_k - \mathbf{x}||^2\right) \\ &= f(\mathbf{x}) + \rho \sum_{k\in\mathcal{R}} \left(||\mathbf{z}_k - \mathbf{x} + \mathbf{u}_k||^2 - ||\mathbf{u}_k||^2\right),\end{aligned}$$

where $\mathbf{u}_k \triangleq \frac{1}{2}\mathbf{y}_k/\rho$ is the scaled dual variable and ρ denotes the penalty when $\mathbf{z}_k \neq \mathbf{x}$. By the alternating direction method of multipliers (ADMM), we can solve (17) by the following iterations with guaranteed convergence [35]:

$$\mathbf{x}^{(t+1)} = \arg\min_{\mathbf{x}} \Gamma(\mathbf{x}, \mathbf{z}_k^{(t)}, \mathbf{u}_k^{(t)}), \tag{18a}$$

$$\mathbf{z}_k^{(t+1)} = \arg\min_{\mathbf{z}_k : |\mathbf{e}_k^H \mathbf{z}_k| \le 1} \Gamma(\mathbf{x}^{(t+1)}, \mathbf{z}_k, \mathbf{u}_k^{(t)}), \tag{18b}$$

$$\mathbf{u}_k^{(t+1)} = \mathbf{u}_k^{(t)} - \mathbf{x}^{(t+1)} + \mathbf{z}_k^{(t+1)}. \tag{18c}$$

The minimization of $\Gamma(\mathbf{x}, \mathbf{z}_k^{(t)}, \mathbf{u}_k^{(t)})$ with respect to $\mathbf{x}$ is an unconstrained problem. Taking the derivative of $\Gamma(\mathbf{x}, \mathbf{z}_k^{(t)}, \mathbf{u}_k^{(t)})$ with respect to $\mathbf{x}$ and letting $\partial\Gamma/\partial\mathbf{x} = \mathbf{0}$, we have

$$\mathbf{x}^{(t+1)} = (\rho K \mathbf{I} - \mathbf{B}\mathbf{B}^H)^{-1} \left(\mathbf{B}^H \mathbf{f}_0 + \rho \sum_{k\in\mathcal{R}} \left(\mathbf{z}_k^{(t)} + \mathbf{u}_k^{(t)}\right)\right),$$

where ρ is chosen properly such that the minimization of $\Gamma(\mathbf{x}, \mathbf{z}_k^{(t)}, \mathbf{u}_k^{(t)})$ is bounded. Given the solution $\mathbf{x}^{(t+1)}$ and $\mathbf{v}_k^{(t+1)} \triangleq \mathbf{x}^{(t+1)} - \mathbf{u}_k^{(t)}$, the optimization of $\mathbf{z}_k$ is a quadratic problem subject to one quadratic constraint $|\mathbf{e}_k^H \mathbf{z}_k| \le 1$:

$$\min_{\mathbf{z}_k} \{||\mathbf{z}_k - \mathbf{v}_k^{(t+1)}||^2 : |\mathbf{e}_k^H \mathbf{z}_k| \le 1\}, \tag{19}$$

which always admits an optimal rank-one solution [31].

Besides the ADMM update procedure, we can also consider a simple heuristic algorithm with reduced complexity based on a practical observation that the direct channel $\mathbf{f}_0$ from the PBS to the DRx-0 is much stronger than the relay channel $\mathbf{b}_k$, i.e., $||\mathbf{f}_0|| \gg ||\mathbf{b}_k||$ for $k \in \mathcal{R}$. This motivates the heuristic design to maximize the projection of $\Gamma_k \mathbf{b}_k$ onto the direct channel $\mathbf{f}_0$ by the choice of complex reflection coefficient, i.e.,

$$\Gamma_k^* = \arg\max_{|\Gamma_k| \le 1} \Gamma_k \mathbf{b}_0^H \hat{\mathbf{f}}_0 = \exp(j \angle \hat{\mathbf{f}}_0^H \mathbf{b}_k).$$

This heuristic can be implemented in a distributed manner at individual relays. Given the shared information $\mathbf{f}_0$, each relay $k \in \mathcal{K}$ estimates the backscatter channel $\mathbf{b}_k$ and aligns the reflection coefficient Γ_k to the projected channel $\hat{\mathbf{f}}_0^H \mathbf{b}_k$.

The feasibility check of (13b) amounts to solve the SDP (16) in line 5 of Algorithm 1. With fixed α and r, it is obvious that the optimal p_s to (16) is given by $\bar{p}_s \triangleq \frac{\bar{r}_2(\alpha,r)}{||\mathbf{B}\mathbf{x}^* + \mathbf{f}_0||^2}$ and the optimal p_e will take its maximum $\bar{p}_e \triangleq \left(e_{\max} - (1-\alpha)\bar{p}_s\right)/\alpha$. Hence, problem (16) can be simplified by

$$\max_{\mathbf{W} \succeq \mathbf{0}} \quad \mathbf{h}_0^H \mathbf{W} \mathbf{h}_0 \tag{20a}$$

$$s.t.\ \mathbf{h}_k^H \mathbf{W} \mathbf{h}_k \ge \bar{p}_b, \quad \forall k \in \mathcal{R}, \tag{20b}$$

$$\mathrm{Tr}(\mathbf{W}) \le \min\left(p_{\max}, \bar{p}_e\right). \tag{20c}$$

If the optimal $\mathbf{W}^*$ happens to be rank-one, the optimal $\hat{\mathbf{w}}^*$ can be recovered from $\mathbf{W}^*$ by eigen-decomposition.

Proposition 1: The SDP (20) *always admits a rank-one solution.*

The proof of Proposition 1 follows a similar approach as that in [36], and we omit the details here for conciseness. For one relay case, e.g., $\mathcal{R} = \{k\}$, the vector $\mathbf{x}$ is degenerated to a complex value $\Gamma_k = |\Gamma_k| e^{j\theta_k}$. Thus, it is optimal to set $|\Gamma_k| = 1$ and θ_k such that

$$\theta_k^* = \arg\max_{\theta_k} (e^{j\theta_k}\mathbf{b}_k)^H \mathbf{f}_0 = \angle \mathbf{f}_0^H \mathbf{b}_k, \tag{21}$$

where $\angle \mathbf{f}_0^H \mathbf{b}_k$ denotes the phase of complex number $\mathbf{f}_0^H \mathbf{b}_k$.

Proposition 2: Assuming that only DTx-k serves as the relay, the optimal rank-one solution $\hat{\mathbf{w}}^*$ *to* (20) *is given by*

$$\hat{\mathbf{w}} = \begin{cases} \hat{\mathbf{h}}_0, & \text{if } \bar{p}_e ||\mathbf{h}_k^H \hat{\mathbf{h}}_0||^2 \geq \bar{p}_b, \\ \beta \hat{\mathbf{h}}_k + \sqrt{1-|\beta|^2}\hat{\mathbf{h}}_k^{\perp}, & \text{otherwise}, \end{cases} \tag{22}$$

where $\beta = \sqrt{\frac{\bar{p}_b}{\bar{p}_e ||\mathbf{h}_k||^2}} \hat{\mathbf{h}}_k^H \hat{\mathbf{h}}_0$, $\hat{\mathbf{h}}_k^{\perp} = \frac{\mathbf{h}_0 - (\hat{\mathbf{h}}_k^H \mathbf{h}_0)\hat{\mathbf{h}}_k}{||\mathbf{h}_0 - (\hat{\mathbf{h}}_k^H \mathbf{h}_0)\hat{\mathbf{h}}_k||}$, *and* $\hat{\mathbf{h}}_k \triangleq \mathbf{h}_k / ||\mathbf{h}_k||$ *is the normalized channel.*

Proof: Without loss of generality, we can focus on the non-trivial case: $\bar{p}_e \leq p_{\max}$. By Proposition 1, we can decompose the solution to (16) as $\mathbf{W} = \bar{p}_e \hat{\mathbf{w}}\hat{\mathbf{w}}^H$, and the proof of Proposition 2 is straightforward by discussing two cases. In the first case, we align $\hat{\mathbf{w}}$ with the channel $\mathbf{h}_0$ to maximize $|\mathbf{h}_0^H \hat{\mathbf{w}}|^2$ without the power constraint (13d). If DTx-k still harvests sufficient energy in this case, i.e., $\bar{p}_e |\mathbf{h}_k^H \hat{\mathbf{w}}|^2 \geq \bar{p}_b$, then $\hat{\mathbf{w}} = \hat{\mathbf{h}}_0$ is the optimal energy beamformer. In the second case with $\bar{p}_e |\mathbf{h}_k^H \hat{\mathbf{h}}_0|^2 < \bar{p}_b$, dedicated energy beamforming is required to power up the relays. We can set the energy beamformer in the form of $\hat{\mathbf{w}} = \beta \hat{\mathbf{h}}_k + \sqrt{1-|\beta|^2}\hat{\mathbf{h}}_k^{\perp}$ [37], where β is a complex coefficient and $\hat{\mathbf{h}}_k^{\perp}$ denotes the normalized projection of $\mathbf{h}_0$ onto the null space of $\mathbf{h}_k$. Thus, we have $\mathbf{h}_k^H \hat{\mathbf{h}}_k^{\perp} = 0$ and $\mathbf{h}_0^H \hat{\mathbf{h}}_k^{\perp} = ||\mathbf{h}_0||^2 - |\mathbf{h}_0^H \hat{\mathbf{h}}_k|^2 \geq 0$. The first part of $\hat{\mathbf{w}}$ ensures $|\mathbf{h}_k^H \hat{\mathbf{w}}|^2 = |\beta \mathbf{h}_k^H \hat{\mathbf{h}}_k|^2 = \bar{p}_b / \bar{p}_e$, and thus $|\beta|^2 = \sqrt{\frac{\bar{p}_b}{\bar{p}_e ||\mathbf{h}_k||^2}}$. Let θ_b be the argument of β, then we have

$$|\mathbf{h}_0^H \hat{\mathbf{w}}|^2 = |||\beta| e^{j\theta_b} \mathbf{h}_0^H \hat{\mathbf{h}}_k + \sqrt{1-|\beta|^2}(||\mathbf{h}_0||^2 - |\mathbf{h}_0^H \hat{\mathbf{h}}_k|^2)||^2.$$

To maximize $|\mathbf{h}_0^H \hat{\mathbf{w}}|^2$, the optimal argument θ_b is given by the conjugate of $\hat{\mathbf{h}}_0^H \hat{\mathbf{h}}_k$, which leads to the result in (22). ■

Algorithm 1 is consisted of a bisection search over the optimal rate r in the outer loop and two SDPs within each iteration, which bring the main computational complexity of Algorithm 1. Nevertheless, the SDP (15) only requires the channel information. Though the SDP (16) or (20) also depends on r within each iteration. The optimal and normalized beamforming vector $\hat{\mathbf{w}}$ to (20) is the same for different r. Hence, we can simply view r as a scaling factor to the power budget constraint in (20c). This implies that we can remove them from the loop and only need to solve them once. By the analytical work in [31], the computational complexity of SDPs (15) and (16) can be evaluated by $O\left(K^{1.5}M^4 + K^{6.5}\right)$, which is reduced comparing to $O\left(K^{2.5}M^4 + K^{6.5}\right)$ of the direct solution to (13). More importantly, the inner loop of Algorithm 1 follows two steps that can be distributed to separated network entities, e.g., the PBS and the DRx-0. This further decreases the instant demand for computational resource at each entity to run Algorithm 1, and also reduces the communication overhead significantly. Specifically, the solution to (15) can be delegated to the DRx-0 and the PBS only collects $\{\mathbf{h}_0, \mathbf{h}_1, \ldots, \mathbf{h}_K\}$ to solve (16). Hence there is no need for the DRx-0 to feed back the channel estimates $\{\mathbf{f}_0, \mathbf{g}\}$ to the PBS. The only information for the DRx-0 to share with the PBS is the relays' optimal reflection coefficients $\mathbf{x}^*$.

C. Adaptive Relay Selection

In previous sections, we assume that the relay set $\mathcal{R}$ is given and fixed in problem (13). Constraint (13d) ensures that all the relays meet the minimum power requirement. If some relay has low EH rate due to its bad channel conditions, e.g., a possibly longer distance to the PBS, the PBS has to spare more channel time (i.e., larger value of α) or higher transmit power to keep it alive, which compromises the overall throughput. This observation motivates us to design a relay selection algorithm that adapts the set of relays to achieve the highest throughput.

Considering a simple case where only one relay is selected to backscatter the PBS' signals, the result in (21) suggests the selection criterion for the optimal relay. Specifically, when we set $\Gamma_k = e^{j\theta_k^*}$ and θ_k^* is given by (21), we have $||\mathbf{B}\mathbf{x} + \mathbf{f}_0||^2 = ||\mathbf{b}_k||^2 + ||\mathbf{f}_0||^2 + 2|\mathbf{f}_0^H \mathbf{b}_k|$. The optimal relay k^* that maximizes $||\mathbf{B}\mathbf{x} + \mathbf{f}_0||^2$ is thus given by

$$k^* = \arg\max_{k \in \mathcal{R}} ||\mathbf{b}_k||^2 + 2|\mathbf{f}_0^H \mathbf{b}_k|. \tag{23}$$

The first term $||\mathbf{b}_k||^2$ in (23) relates to the channel $\mathbf{h}_k$ from the PBS to the DTx-k and the backscatter channel g_k from the DTx-k to the DRx-0. Larger $||\mathbf{b}_k||^2$ implies that the relay is closer to both of the PBS and the DRx-0, or the channels $\mathbf{h}_k$ and g_k are highly correlated. The second term in (23) accounts for the correlation between the relay channel $\mathbf{b}_k$ and the direct channel $\mathbf{f}_0$. Multiple relays can enhance the signal strength at the targeted receiver by a joint design of their reflection coefficients. However, the optimal selection of multiple relays amounts to a combinatorial problem. A simple heuristic is to select the relays one by one according to the selection criterion in (23). Though this heuristic is simple and easy to implement, it fails to provide performance guarantee as it neglects the correlations between different relay channels.

In this part, we design an adaptive relay algorithm that not only determines the relays' optimal operating parameters, but also finds the optimal set of relays in an iterative process. Let $z_k \in \{0, 1\}$ indicate whether DTx-k serves as the relay, then we can rewrite (13c) as $p_s ||\mathbf{B}\mathrm{D}(\mathbf{z})\mathbf{x} + \mathbf{f}_0||^2 \geq \bar{\gamma}_2(\alpha, r)$, where $\mathbf{B}\mathrm{D}(\mathbf{z}) = [\mathbf{b}_1 z_1, \mathbf{b}_2 z_2, \ldots, \mathbf{b}_K z_K]$. When some relay is not selected, e.g., $z_k = 0$, the relay channel $\mathbf{b}_k$ will have no contribution to the data rate in the second hop. The proposed relay selection algorithm is to adapt the indicator $\mathbf{z}$ iteratively as detailed in Algorithm 2. The algorithm starts from the simplest case with no relays joining in the transmission. Thus, the rate constraint (13c) is simplified as $||\mathbf{f}_0||^2 \geq \bar{\gamma}_2(\alpha, r)$ and the optimal energy beamformer is aligned with the channel $\mathbf{h}_0$ to maximize the data rate in the first hop. Given the solution to this special case, we can check the energy levels of all the relays and take the one with the highest energy level (i.e., DTx-k^* in line 7 of Algorithm 2) into the set $\mathcal{R}^{(t)}$.

Algorithm 2 Adaptive Relay Selection Algorithm

Input: The relays' power demand p_b and parameter α
Output: The PBS' beamforming strategy $(\hat{\mathbf{w}}^{(t)}, \hat{\mathbf{v}}^{(t)})$ and the set of relays $\mathcal{R}^{(t)}$ at convergence
1: Initialize $r_{\max}$, $r_{\min}$, $\mathcal{R}^{(0)} = \emptyset$, and $r^{(0)} = 0$
2: $\hat{\mathbf{w}}^{(t)} \leftarrow \mathbf{h}_0/||\mathbf{h}_0||$, $\hat{\mathbf{v}}^{(t)} \leftarrow \mathbf{f}_0/||\mathbf{f}_0||$ for $t = 1$
3: Check feasibility of $p_e|\mathbf{h}_0^H \hat{\mathbf{w}}^{(t)}|^2 \geq \bar{\gamma}_1(\alpha, r^{(t)})$ and $||\mathbf{f}_0||^2 \geq \bar{\gamma}_2(\alpha, r^{(t)})$ for fixed α and $r^{(t)}$
4: Update $r^{(t)}$ in a bisection method until convergence
5: **while** $r^{(t)} - r^{(t-1)} \geq \epsilon$
6: $t \leftarrow t + 1$
7: $k^* \leftarrow \arg\max_{k \in \mathcal{N} \setminus \mathcal{R}^{(t-1)}} |\mathbf{h}_k^H \hat{\mathbf{w}}^{(t-1)}|^2$
8: $\mathcal{R}^{(t)} \leftarrow \mathcal{R}^{(t-1)} \cup \{k^*\}$
9: Maximize r with the relay set $\mathcal{R}^{(t)}$ by Algorithm 1
10: **if** $r > r^{(t-1)}$ **then** $r^{(t)} \leftarrow r$ **else** $\mathcal{R}^{(t)} \leftarrow \mathcal{R}^{(t-1)} \setminus \{k^*\}$ and $r^{(t)} \leftarrow r^{(t-1)}$, **end if**
11: **end while**
12: Return $\hat{\mathbf{w}}^{(t)}$, $\hat{\mathbf{v}}^{(t)}$, $\mathcal{R}^{(t)}$, and $r^{(t)}$

Then, we solve the throughput maximization problem (13) by Algorithm 1 with the fixed relay set $\mathcal{R}^{(t)}$. If the new relay set $\mathcal{R}^{(t)}$ improves the effective throughput, we accept DTx-k^* as the relay and update the throughput performance, otherwise we remove DTx-k^* from the set $\mathcal{R}^{(t)}$ and keep current relay strategy unchanged. The algorithm iterates until the throughput performance cannot be improved any more. Note that the number of updates in Algorithm 2 is linear to the total number of relays. Each update is determined by an evaluation of the relay performance in Algorithm 1 with fixed relay set $\mathcal{R}$. Hence, we can derive the overall computational complexity of Algorithm 2 as $O\left(K^{2.5}M^4 + K^{7.5}\right)$.

IV. Robust Relay Backscatter Communications

The solution to problem (13) requires the channel information $\{\mathbf{f}_0, \mathbf{h}_k, g_k\}$, which relies on channel estimations at the DUEs and the PBS. In practice, channel estimation is a power-consuming operation that prevents the relays and the targeted receiver from frequent channel estimations. Besides, the channel estimation is usually unreliable due to limited or untimely information exchange between the transceivers. In the sequel, we reformulate and solve the robust counter-parts of (13) with different levels of uncertain channel information.

A. Robust Against the Backscatter Channel

The PBS has constant energy supply and more computation resource than that of the low power DUEs. Thus it can perform frequent estimations of the channels $\mathbf{f}_0$ and $\mathbf{h}_k$, while the estimation of the backscatter channel $\mathbf{g}$ is left to the resource constrained DRx-0. Hence, we assume that the channels $\mathbf{f}_0$ and $\mathbf{h}_k$ can be obtained with high accuracy, while the estimation of g_k is error-prone. Specifically, the error estimate of $\mathbf{g}$ is assumed to be bounded by $\delta_{\mathbf{g}}$, which allows us to define the uncertainty of $\mathbf{g}$ as follows:

$$\mathbb{U}_{\mathbf{g}} \triangleq \{\mathbf{g} \in \mathbb{C}^K | \mathbf{g} = \bar{\mathbf{g}} + \mathbf{d} \text{ and } \mathbf{d}^H\mathbf{d} \leq \delta_{\mathbf{g}}^2\}, \tag{24}$$

where $\bar{\mathbf{g}}$ and $\mathbf{d}$ denote the nominal and error estimates of channel $\mathbf{g}$, respectively. As the uncertain channel g_k only presents in (13c), we focus on deriving the robust counterpart of (13c) as follows:

$$p_s||\mathbf{H}\mathrm{D}(\mathbf{g})\mathbf{x} + \mathbf{f}_0||^2 \geq \bar{\gamma}_2(\alpha, r), \quad \forall \mathbf{g} \in \mathbb{U}_{\mathbf{g}}. \tag{25}$$

Let $\Delta = \mathrm{D}(\mathbf{d})$. Then we have $\mathrm{D}(\mathbf{g}) = \mathrm{D}(\bar{\mathbf{g}}) + \Delta$ and require

$$\mathbf{Tr}(\Delta^H \mathbf{H}_s \Delta \mathbf{X}) + 2\mathbf{Tr}\big(\mathrm{Re}(\Delta^H \mathbf{G})\big) + ||\bar{\mathbf{f}}_{\mathbf{x}}||^2 \geq \bar{\gamma}_2/p_s \tag{26}$$

holds with any $\mathbf{g} \in \mathbb{U}_{\mathbf{g}}$, where $\mathbf{H}_s \triangleq \mathbf{H}^H\mathbf{H}$. Here we define $\bar{\mathbf{f}}_{\mathbf{x}} \triangleq \bar{\mathbf{B}}\mathbf{x} + \mathbf{f}_0$ and $\mathbf{G} \triangleq \mathbf{H}^H\bar{\mathbf{f}}_{\mathbf{x}}\mathbf{x}^H = \mathbf{H}^H\bar{\mathbf{B}}\mathbf{X} + \mathbf{H}^H\mathbf{f}\mathbf{x}^H$ with the nominal channel matrix $\bar{\mathbf{B}}$ given by $\mathbf{H}\mathrm{D}(\bar{\mathbf{g}})$. Let $\mathrm{vec}(\cdot)$ denote the operation of cascading all vectors of a matrix into one vector. Note that $\mathbf{Tr}(\mathbf{A}^H\mathbf{B}) = \mathrm{vec}(\mathbf{A})^H\mathrm{vec}(\mathbf{B})$ and $\mathrm{vec}(\mathbf{ABC}) = (\mathbf{C}^H \otimes \mathbf{A})\mathrm{vec}(\mathbf{B})$. Then we can rewrite (26) as

$$\mathrm{vec}(\Delta)^H\mathbf{H}_{\mathbf{x}}\mathrm{vec}(\Delta) + 2\mathrm{Re}\left(\mathrm{vec}(\Delta)^H\mathrm{vec}(\mathbf{G})\right) + ||\bar{\mathbf{f}}_{\mathbf{x}}||^2 \geq \bar{\gamma}_2/p_s, \quad \forall \mathrm{vec}(\Delta)^H\mathbf{Q}\mathrm{vec}(\Delta) \leq \delta_{\mathbf{g}}^2, \tag{27}$$

where $\mathbf{H}_{\mathbf{x}} \triangleq \mathbf{X} \otimes \mathbf{H}_s$ and $\mathbf{Q} \triangleq \begin{bmatrix} \mathbf{I}_{N-1} \otimes \mathbf{e}_1 & \mathbf{0} \\ \mathbf{0} & 1 \end{bmatrix}$ with $\mathbf{e}_1 = [1, 0, 0, \cdots, 0]^T$. By the S-lemma [38], we can transform (27) into a linear matrix inequality:

$$\begin{bmatrix} \mathbf{H}_{\mathbf{x}} + \tau\mathbf{Q} & \mathrm{vec}(\mathbf{G}) \\ \mathrm{vec}(\mathbf{G})^H & ||\bar{\mathbf{f}}_{\mathbf{x}}||^2 - \bar{\gamma}_2/p_s - \tau\delta_{\mathbf{g}}^2 \end{bmatrix} \succeq 0, \tag{28}$$

where $\tau \geq 0$. Hence, for fixed power allocation (p_e, p_s), the robust relay strategy can be found by the following problem:

$$\max_{r, \mathbf{W}, \mathbf{X}, \mathbf{x}} \{r : \text{ (13b), (13d)} - \text{(13e), (28)}\}. \tag{29}$$

Problem (29) only revises (13c) and hence Proposition 1 still holds for (29), i.e., the optimal $\mathbf{W}^*$ to (29) is always rank-one.

The rank-one approximation of $\mathbf{x}$ can be extracted by a similar approach for (15). In particular, to ensure the feasibility of (26), we can evaluate a max-min problem as follows:

$$\max_{\mathbf{X}, \mathbf{x}} \min_{\Delta} \mathbf{Tr}(\Delta^H \mathbf{H}_s \Delta \mathbf{X}) + 2\mathbf{Tr}\big(\mathrm{Re}(\Delta^H \mathbf{G})\big) + ||\bar{\mathbf{f}}_{\mathbf{x}}||^2, \tag{30}$$

and compare its objective value to $\bar{\gamma}_2/p_s$. Given the solution $\mathbf{X}^*$ to the SDR (29), we can determine the worst-case Δ^* by solving the inner minimization of (30). It is easy to show that the inner minimization is a convex problem and thus Δ^* is efficiently tractable. Once we obtain the worst-case error estimate $\mathbf{d}^* = \mathrm{diag}(\Delta^*)$, the worst-case backscatter channel is given by $\mathbf{g}^* = \bar{\mathbf{g}} + \mathbf{d}^*$. Then, fixing $\mathbf{B}^* = \mathbf{H}\mathrm{D}(\mathbf{g}^*)$, we can extract the rank-one approximation of $\mathbf{X}$ by solving the outer maximization of (30) in a similar approach for (15).

B. Robust Against the Relay Channels

We further consider a more general case in which both $\mathbf{h}_k$ and g_k are subject to unknown error estimates. In particular, the error estimate $\hat{\mathbf{h}}_k$ of the channel $\mathbf{h}_k$ for $k \in \{0\} \cup \mathcal{R}$ is bounded and confined in a convex set defined as follows:

$$\mathbb{U}_k \triangleq \{\mathbf{h}_k \in \mathbb{C}^M | \mathbf{h}_k = \bar{\mathbf{h}}_k + \hat{\mathbf{h}}_k \text{ and } \hat{\mathbf{h}}_k^H\hat{\mathbf{h}}_k \leq \delta_k^2\}, \tag{31}$$

where $\bar{\mathbf{h}}_k$ denotes the nominal channel estimate of $\mathbf{h}_k$. When both $\mathbf{h}_k$ and g_k are subject to uncertainties, (13c) involves a

complicated biquadratic form [39]. To bypass this difficulty, we note that the received signal at DRx-0 is a joint effect of $\mathbf{h}_k$ in the first hop and g_k in the second hop, and therefore we focus on the uncertainty of the equivalent relay channel $\mathbf{b}_k = g_k\mathbf{h}_k$, instead of characterizing the uncertainties of $\mathbf{h}_k$ and g_k separately. Specifically, we model the uncertainty of $\mathbf{B} = [\mathbf{b}_1, \mathbf{b}_2, \ldots, \mathbf{b}_K] \in \mathbb{C}^{M\times K}$ in Frobenius norm:

$$\mathbb{U}_{\mathbf{b}} \triangleq \left\{\bar{\mathbf{B}} + \Delta_{\mathbf{b}} : ||\Delta_{\mathbf{b}}||_F^2 = \mathbf{Tr}(\Delta_{\mathbf{b}}\Delta_{\mathbf{b}}^H) \le \delta_{\mathbf{b}}^2\right\}, \quad (32)$$

where $\bar{\mathbf{B}}$ denotes the nominal channel estimate and $\delta_{\mathbf{b}}$ is the upper bound of error estimate $\Delta_{\mathbf{b}}$.

Proposition 3: Given the uncertainties of $\mathbf{h}_k$ *and* $\mathbf{B}$ *in* (31) *and* (32)*, respectively, the robust counter-part of* (13) *has the following equivalence:*

$$\max_{r,\mathbf{W},\mathbf{X},\mathbf{x}} \; r \quad (33a)$$

$$s.t. \begin{bmatrix} \mathbf{W} + t_0\mathbf{I} & \mathbf{W}\bar{\mathbf{h}}_0 \\ \bar{\mathbf{h}}_0^H\mathbf{W} & \bar{\mathbf{h}}_0^H\mathbf{W}\bar{\mathbf{h}}_0 - \bar{\gamma}_1/p_e - t_0\delta_0^2 \end{bmatrix} \ge 0, \quad (33b)$$

$$\begin{bmatrix} \mathbf{W} + t_k\mathbf{I} & \mathbf{W}\bar{\mathbf{h}}_k \\ \bar{\mathbf{h}}_k^H\mathbf{W} & \bar{\mathbf{h}}_k^H\mathbf{W}\bar{\mathbf{h}}_k - \bar{p_b}/p_e - t_k\delta_k^2 \end{bmatrix} \ge 0, \quad (33c)$$

$$\begin{bmatrix} \mathbf{X}\otimes\mathbf{I} + \tau\mathbf{I} & \mathrm{vec}(\bar{\mathbf{f}}_{\mathbf{x}}\mathbf{x}^H) \\ \mathrm{vec}^H(\bar{\mathbf{f}}_{\mathbf{x}}\mathbf{x}^H) & ||\bar{\mathbf{f}}_{\mathbf{x}}||^2 - \bar{\gamma}_2/p_s - \tau\delta_{\mathbf{b}}^2 \end{bmatrix} \ge 0, \quad (33d)$$

$$(13e),\ \tau \ge 0, t_0 \ge 0, t_k \ge 0, k \in \mathcal{R}. \quad (33e)$$

Proof: The proof of Proposition 3 relies on convex reformulations of the robust counter-parts of (13b)-(13d). The constraints (13b) and (13d) are perturbed by $\mathbf{h}_k = \bar{\mathbf{h}}_k + \hat{\mathbf{h}}_k$. The robust counter-part of (13b) is given by

$$\hat{\mathbf{h}}_0^H\mathbf{W}\hat{\mathbf{h}}_0 + \hat{\mathbf{h}}_0^H\mathbf{W}\bar{\mathbf{h}}_0 + \bar{\mathbf{h}}_0^H\mathbf{W}\hat{\mathbf{h}}_0 + \bar{\mathbf{h}}_0\mathbf{W}\bar{\mathbf{h}}_0 - \bar{\gamma}_1/p_e \ge 0, \quad \forall \hat{\mathbf{h}}_0^H\hat{\mathbf{h}}_0 \le \delta_0^2,$$

which can be rewritten in a linear matrix inequality (33b) by the S-lemma. A similar result applies to (13d) and we can obtain the equivalence in (33c). Then we focus on the convex reformulation of (13c) when the relay channel $\mathbf{B}$ is subject to uncertainty (32). Given $\mathbf{B} = \bar{\mathbf{B}} + \Delta_{\mathbf{b}}$, we require

$$||\mathbf{B}\mathbf{x} + \mathbf{f}_0||^2 = ||\bar{\mathbf{f}}_{\mathbf{x}}||^2 + \mathrm{vec}(\Delta_{\mathbf{b}})^H(\mathbf{X}\otimes\mathbf{I})\mathrm{vec}(\Delta_{\mathbf{b}}) + 2\mathrm{Re}\Big(\mathrm{vec}(\Delta_{\mathbf{b}})^H\mathrm{vec}(\bar{\mathbf{f}}_{\mathbf{x}}\mathbf{x}^H)\Big) \ge \bar{\gamma}_2/p_s \quad (34)$$

holds for any $\Delta_{\mathbf{b}}$ such that $\mathrm{vec}(\Delta_{\mathbf{b}})^H\mathrm{vec}(\Delta_{\mathbf{b}}) \le \delta_{\mathbf{b}}^2$. Applying the S-lemma again, we can rewrite (34) into the semi-definite representation (33d). ∎

C. Robust Power Allocation and Relay Selection

We can solve (33) efficiently with fixed power allocation (p_e, p_s). The rank-one approximation of $\mathbf{X}^*$ can be extracted by a similar approach as that for the robust problem (29). To extract $\hat{\mathbf{w}}^*$ from the optimal $\mathbf{W}^*$ to (33), we first determine the worst-case channel estimates by

$$\hat{\mathbf{h}}_k^* = \arg\min_{\hat{\mathbf{h}}_k^H\hat{\mathbf{h}}_k \le \delta_k^2} (\bar{\mathbf{h}}_k + \hat{\mathbf{h}}_k)^H\mathbf{W}^*(\bar{\mathbf{h}}_k + \hat{\mathbf{h}}_k).$$

That is, $\hat{\mathbf{h}}_k^* = -(\mathbf{W}^* + \lambda_k\mathbf{I})^{-1}\mathbf{W}^*\bar{\mathbf{h}}_k$ and λ_k denotes the dual variable such that $||\hat{\mathbf{h}}_k^*|| = \delta_k$. Then, we can solve the SDP (16) with the fixed $\hat{\mathbf{h}}_k^*$ and $\mathbf{h}_k = \bar{\mathbf{h}}_k + \hat{\mathbf{h}}_k^*$, which always admits a rank-one solution by Proposition 1. The joint optimization of the power allocation (p_e, p_s) and the relay strategy can be performed by alternating optimization, as illustrated in Algorithm 3. Given a fixed power allocation $(p_e^{(t)}, p_s^{(t)})$, we first solve the SDP (33) with the optimal solution given by $\mathbf{O}^{(t)}$, which constitutes the main computational complexity of Algorithm 3, denoted as $O\left(K^7M^3 + K^3M^7\right)$ by the analysis in [32]. After that, we fix $\mathbf{O}^{(t)}$ and solve (33) to update $(p_e^{(t+1)}, p_s^{(t+1)})$. This iteration is guaranteed to converge as it improves the throughput performance in every step.

Algorithm 3 Robust Backscatter Relay Strategy

Input: The channel uncertainties of $\mathbf{h}_k$ and $\mathbf{B}$
Output: The beamformer $\mathbf{w}$, power allocation (p_e, p_s), and reflection coefficient $\mathbf{x}$

1: Initialize $(p_e^{(t)}, p_s^{(t)})$ and $\mathrm{d}r^{(t)} = 1$ for $t = 0$
2: **while** $\mathrm{d}r^{(t)} \ge \epsilon$
3: Find solution $\mathbf{O}^{(t+1)}$ to (33) with fixed $(p_e^{(t)}, p_s^{(t)})$
4: Update $(p_e^{(t+1)}, p_s^{(t+1)})$ by solving (33) with $\mathbf{O}^{(t+1)}$
5: $\mathrm{d}r^{(t+1)} \leftarrow r^{(t+1)} - r^{(t)}$
6: $t \leftarrow t + 1$
7: **end while**

The robust relay selection under uncertain channel information follows a similar procedure as that in Algorithm 2 with minor modifications. The initialization of energy beamformer $\hat{\mathbf{w}}^{(t)}$ has to account for the uncertainty in $\mathbf{h}_0$. Thus, it is obtained through the worst-case rate maximization:

$$\hat{\mathbf{w}}^{(1)} = \arg\max_{||\hat{\mathbf{w}}||\le 1} \min_{\hat{\mathbf{h}}_0^H\hat{\mathbf{h}}_0 \le \delta_0^2} |(\bar{\mathbf{h}}_0 + \hat{\mathbf{h}}_0)^H\hat{\mathbf{w}}|^2.$$

Note that $|(\bar{\mathbf{h}}_0 + \hat{\mathbf{h}}_0)^H\hat{\mathbf{w}}| \ge ||\bar{\mathbf{h}}_0^H\hat{\mathbf{w}}| - |\hat{\mathbf{h}}_0^H\hat{\mathbf{w}}|| \ge ||\bar{\mathbf{h}}_0^H\hat{\mathbf{w}}| - \delta_0||\hat{\mathbf{w}}||$. Assuming that δ_0 is small compared to $||\bar{\mathbf{h}}_0||$, we simply have $\hat{\mathbf{w}}^{(1)} = \arg\max_{||\hat{\mathbf{w}}||\le 1} |\bar{\mathbf{h}}_0^H\hat{\mathbf{w}}|^2 = \bar{\mathbf{h}}_0/||\bar{\mathbf{h}}_0||$. That is, the initial energy beamformer is aligned to the nominal channel estimate $\bar{\mathbf{h}}_0$. Correspondingly, the relay selection in line 7 of Algorithm 2 is replaced by

$$k^* = \arg\max_{k\in\mathcal{N}\setminus\mathcal{R}^{(t-1)}} \min_{\hat{\mathbf{h}}_k^H\hat{\mathbf{h}}_k \le \delta_k^2} |(\bar{\mathbf{h}}_k + \hat{\mathbf{h}}_k)^H\hat{\mathbf{w}}^{(t-1)}|^2 = \arg\max_{k\in\mathcal{N}\setminus\mathcal{R}^{(t-1)}} |\bar{\mathbf{h}}_k^H\hat{\mathbf{w}}^{(t-1)} - \delta_k|^2.$$

Based on the relay set $\mathcal{R}^{(t)}$, the robust throughput can be obtained by solving (33) in Algorithm 3.

V. Numerical Results

The numerical evaluations contain three parts. Firstly, we verify the convergence and performance of the power allocation and the relay strategy in Algorithm 1, given a fixed set of backscatter relays. Secondly, we consider channel uncertainties due to estimation errors and evaluate the robust throughput performance of the backscatter relay communications. In the third part, by varying the set of relays, we observe that the optimal throughput changes significantly due to the relays' different channel conditions. This observation motivates us to design an adaptive algorithm to update the set of relays and achieve the highest throughput. In the experiments,

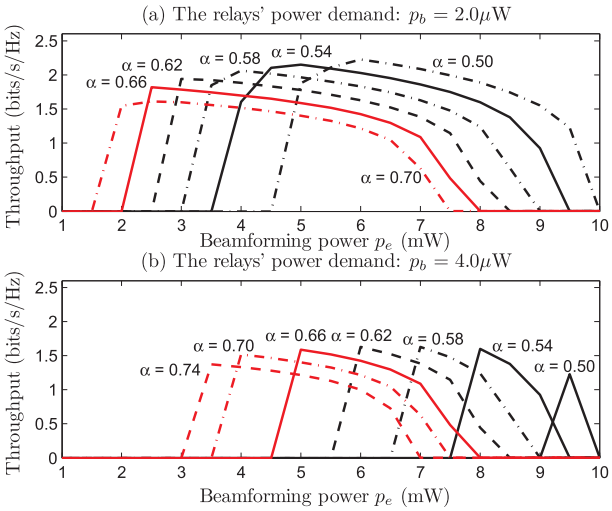

Fig. 3. The throughput as a function of the beamforming power p_e.

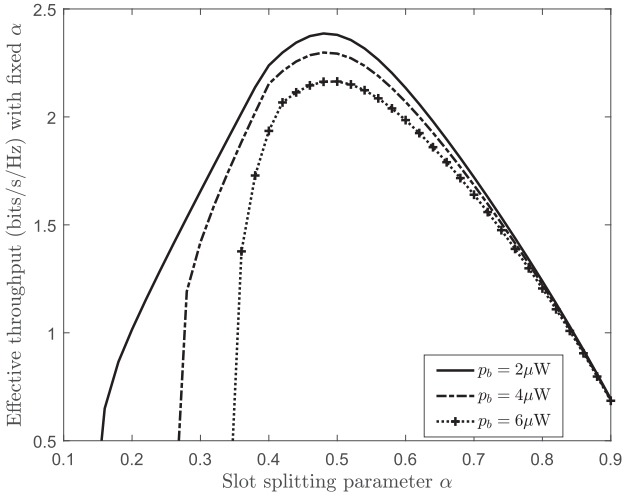

(a) Concavity of throughput in the parameter α.

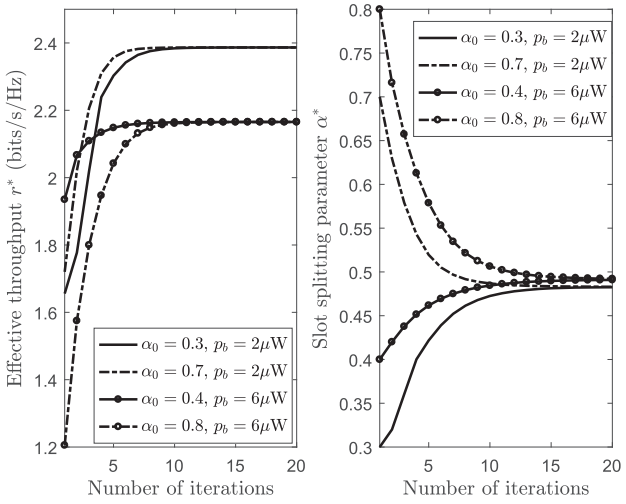

(b) Convergence to the optimal α^* and throughput r^*.

Fig. 4. Efficient search for (α^*, r^*) optimal to (11).

without loss of generality, we consider 3 DUEs as the relays for the transceiver pair DTx/DRx-0. The distance in meters between the PBS and the DTx/DRx-0 is set to 2 and 6, respectively. To differentiate the relays, we set the distances from the PBS to the relays as the vector $\mathbf{d} = [2, 3, 4]$. Under this setting, we observe that the DTx-1 is closest to the PBS while the DTx-3 has the largest distance to the PBS. The distance between each relay and the DRx-0 is the same and set to 4. The path loss exponent is set to 2 and the path loss measured at 1 meter distance is set to -30dB. The noise power is -100dBm and the PBS' maximum transmit power is $p_{\max} = 10$mW. The RF energy conversion coefficient is $\eta = 0.5$ and the total energy available in a time slot is constrained by $e_{\max} = 5$mJ.

A. Problem Structure and Algorithm Convergence

We first show the throughput in (11) by a greedy search over the beamforming power p_e in the first hop. For each fixed p_e, we evaluate the optimal throughput in the SDP (13). By examining the results, we can verify some properties of the problem (11). As shown in Fig. 3, each curve corresponds to the effective throughput as a function of p_e with a fixed slot splitting parameter α. We fairly observe that each curve shows a *concave structure* over the beamforming power p_e. The optimal p_e^* corresponding to the peak throughput on each curve is generally decreasing with the increase of α, e.g., $p_e^* \approx 4.0$ for $\alpha = 0.58$ and $p_e^* \approx 3$ for $\alpha = 0.62$ as shown in Fig. 3(a). That is, when α is small, the PBS has to increase its beamforming power in the first hop to ensure sufficient power transfer to the relays. Moreover, the PBS also needs to increase p_e^* when the relays' power demand p_b increases, e.g., we require $p_e \geq 3.0$ when $p_b = 2.0$ as shown in Fig. 3(a) and $p_e \geq 6.5$ when $p_b = 4$ as shown in Fig. 3(b) to power up all the cooperative relays with the parameter α set to 0.58. Once all the relays in $\mathcal{R}$ become active, the effective throughput may increase as shown in the cases of $\alpha \in \{0.50, 0.54, 0.58\}$ in Fig. 3(a) when we further increase the beamforming power p_e. These observations imply that the throughput bottleneck lies in the first hop. As p_e further increases, the effective throughput may even decrease for some other cases, e.g., $\alpha \in \{0.62, 0.66, 0.70\}$ as shown in Fig. 3(b). That is, the bottleneck shifts to the second hop with either larger α or higher transmit power p_e in the first hop.

In Fig. 4, we numerically show that the optimal throughput obtained from problem (11) has a concave structure in parameter α, which motivates the gradient-based search for the optimal parameter α^*. When α is small, the PBS is unable to power up the relays and hence the problem (11) becomes infeasible. For larger power demand p_b, the minimum α ensuring the feasibility of (11) also becomes larger, as shown in Fig. 4(a). When α becomes large, the effective throughput will decrease due to reduced transmission time in the second hop. In Fig. 4(b), we show the convergent throughput r and the parameter α resulting from the search algorithm with different p_b and initial value of α, e.g., the throughput converges to the same optimal value 2.4 when we set $\alpha_0 = 0.3$ and $\alpha_0 = 0.7$ as the initial value, respectively. In the outer loop, we employ the gradient-based method to search for the

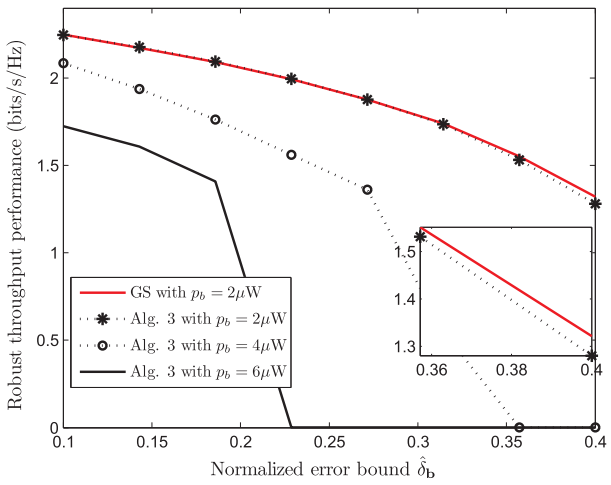

Fig. 5. Robust throughput with uncertain channel information.

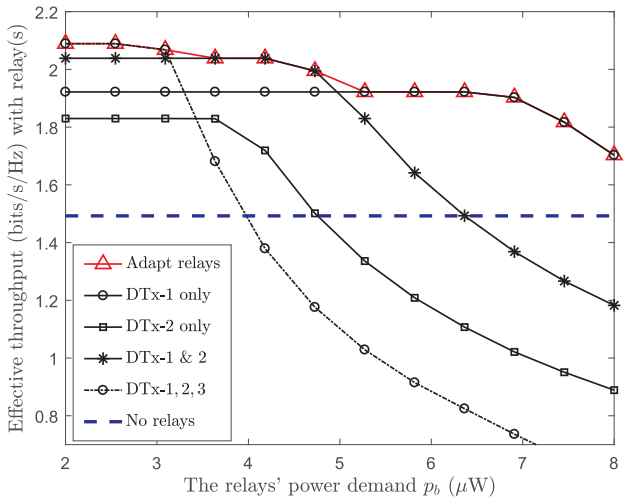

Fig. 6. Effective throughput in different relay strategies.

optimal α^*, which can be very efficient as the total number of iterations till convergence is less than 20 in our simulation settings. Within each iteration, we employ Algorithm 1 to determine the optimal throughput r^* in a bisection method. Fig. 4(b) corroborates the intuition that the optimal throughput decreases and α^* increases with a higher power demand p_b at the backscatter relays.

B. Robust Performance With Channel Uncertainty

In Fig. 5, we show the robust throughput performance when both of the channels $\mathbf{h}_k$ and $\mathbf{b}_k$ are subject to uncertainties in (31) and (32), respectively. Without loss of generality, we fix the set of relays as $\mathcal{R} = \{1, 2\}$ and assume that $\delta_1 = \delta_2 = \delta_0$. By varying the normalized error bound $\hat{\delta}_{\mathbf{b}} = \delta_{\mathbf{b}}/||\mathbf{b}||$, we record the dynamics of the robust throughput performance with different power demands at the backscatter relays. It is obvious that the robust throughput is decreasing with the increase of $\delta_{\mathbf{b}}$. A larger error bound implies that the channel estimation is prone to have larger errors. As such, the throughput estimation becomes more conservative or even becomes zero, as shown in Fig. 5 for the cases with large power demand p_b. This means that we may not guarantee a nonnegative throughput performance with a quite large error estimate of the backscatter channel. To validate the performance of Algorithm 3, we also plot the globally optimal throughput by a greedy search (GS) algorithm in Fig. 5. The GS algorithm iterates over all feasible points of the power allocation (p_e, p_s) and evaluates the optimal solution to the SDP (33) efficiently at each point. We observe that the alternating optimization in Algorithm 3 actually performs relatively well, achieving very close performance to the optimum.

C. Adapting the Set of Backscatter Relays

Due to the relays' different channel conditions, the fixed relay strategy cannot achieve a balance between wireless energy transfer and information transmission. For example, DTx-3 is far away from the PBS and thus it requires a longer charging time α and higher beamforming power p_e to keep alive. If DTx-3 joins in the set of relays, its bad channel condition will severely limit the overall channel capacity due to the reduced channel time and transmit power in the second hop. This observation motivates us to adapt the set of relays to achieve the maximum effective throughput. In Fig. 6, we show the optimal throughput with different relay strategies. For a better comparison, we show the case of no passive relays assisting the data transmissions. We note that, the effective throughput is generally higher if some DTx with better channel is selected as the relay. In particular, DTx-1 provides much better throughput than that of DTx-2 as DTx-1 is closer to the PBS. Besides, we observe that multiple relays are not necessarily better than one relay. When all relays have sufficient energy, we can achieve a cooperative gain by employing more relays in the transmission. However, multi-relay cooperation becomes worse off when the PBS' energy beamforming becomes inefficient to power up all the relays. As shown in Fig. 6, when $p_b \geq 5$, the joint effort of DTx-1 and DTx-2 is worse than that is solely achieved by DTx-1. We observe that the backscatter relay strategy significantly improves the throughput when the relays' power demand is low. However, when power demand is high, the PBS will spare more beamforming energy to power up the relays with the cost of decrease in throughput.

Another common observation from Fig. 6 is that, the effective throughput is kept constant initially but experiencing a sudden drop when the relays' power demand p_b is beyond a threshold value, namely, the cut-off point. When p_b is small, the relays are easily fulfilled by the PBS' WPT with the beamformer $\hat{\mathbf{w}}$ aligned to the channel $\hat{\mathbf{h}}_0$. The cut-off point occurs when $\hat{\mathbf{w}} = \hat{\mathbf{h}}_0$ fails to power up some of the relays. In this case, the PBS will optimize a new energy beamformer to increase energy transfer to the dying relays, which causes a significant drop in the throughput as shown in Fig. 6. Correspondingly, a larger α is also required to transfer sufficient energy to the relays as shown in Fig. 7. A counter-intuitive observation is that the beamforming power p_e drops significantly when p_b is beyond the cut-off point as shown in Fig. 8. This implies that, to improve the effective throughput, it will be more efficient to prolong the charging time than increase the transmit power at the PBS.

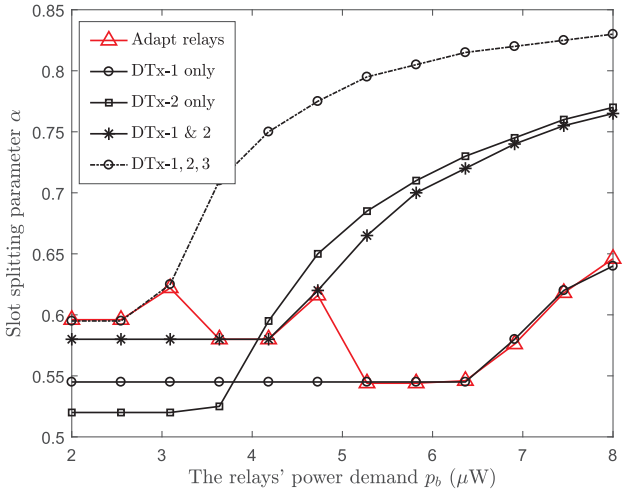

Fig. 7. The optimal α increases with the relays' power demand p_b.

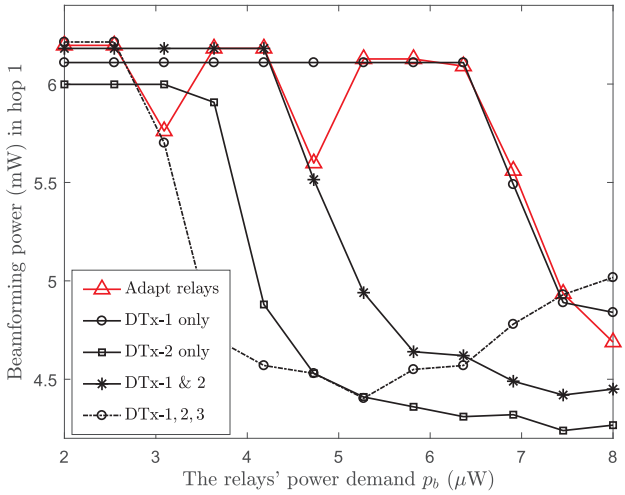

Fig. 8. The beamforming power vs. the relays' power demand p_b.

In Fig. 6, we also show the throughput performance of the adaptive relay selection algorithm. When p_b is small, multiple relays are selected by Algorithm 2 to contribute a higher throughput for DTx/DRx-0, i.e., DTx-1, DTx-2 and DTx-3 all join in the relay set $\mathcal{R}$. When p_b is larger, it is preferred to reduce the number of relays. Noting that DTx-3 has the worst channel condition, it is firstly kicked out from the relay set $\mathcal{R}$. DTx-2 is also kicked out when p_b is beyond 5 as shown in Fig. 6. The optimal α is reduced each time Algorithm 2 updates the relay strategy as shown in Fig. 7. That is because, the relays' channel conditions critically affect their availability when p_b increases. Once we drop the relays with the bad channel conditions, we can improve the efficiency in energy transfer and thus the charging time can be reduced.

VI. Conclusions

In this work, we consider a relay network with multiple low power backscatter radios. Motivated by the observation that the backscatter radios' power demand can be easily fulfilled by WPT, they are willing to serve as wireless relays for each other. The new features of backscatter communication urge a redesign of the WPT and transmission control schemes. To fulfill this objective, we have proposed a two-hop backscatter relay protocol and formulated a throughput maximization problem. We further notice that the channel estimation is power-consuming and thus a difficult task for the low power backscatter radios. Without frequent channel estimations, accurate channel information becomes unavailable. To take account of the channel uncertainties, we have introduced a robust counter-part of the throughput maximization problem and proposed a simple heuristic to maximize the robust performance by alternating optimization.

References

[1] D. Niyato, D. I. Kim, M. Maso, and Z. Han, "Wireless powered communication networks: Research directions and technological approaches," *IEEE Wireless Commun.*, vol. 24, no. 6, pp. 88–97, Dec. 2017.
[2] I. Krikidis, S. Timotheou, S. Nikolaou, G. Zheng, D. W. K. Ng, and R. Schober, "Simultaneous wireless information and power transfer in modern communication systems," *IEEE Commun. Mag.*, vol. 52, no. 11, pp. 104–110, Nov. 2014.
[3] X. Lu, P. Wang, D. Niyato, D. I. Kim, and Z. Han, "Wireless networks with RF energy harvesting: A contemporary survey," *IEEE Commun. Surveys Tuts.*, vol. 17, no. 2, pp. 757–789, 2nd Quart., 2015.
[4] C. Boyer and S. Roy, "Backscatter communication and RFID: Coding, energy, and MIMO analysis," *IEEE Trans. Commun.*, vol. 62, no. 3, pp. 770–785, Mar. 2014.
[5] V. Liu, A. Parks, V. Talla, S. Gollakota, D. Wetherall, and J. R. Smith, "Ambient backscatter: Wireless communication out of thin air," in *Proc. ACM SIGGOMM*, Aug. 2013, pp. 39–50.
[6] A. N. Parks, A. Liu, S. Gollakota, and J. R. Smith, "Turbocharging ambient backscatter communication," in *Proc. ACM SIGGOMM*, Aug. 2014, pp. 619–630.
[7] D. Bharadia, K. R. Joshi, M. Kotaru, and S. Katti, "BackFi: High throughput WiFi backscatter," in *Proc. ACM SIGCOMM*, 2015, pp. 283–296.
[8] A. A. Nasir, X. Zhou, S. Durrani, and R. A. Kennedy, "Relaying protocols for wireless energy harvesting and information processing," *IEEE Trans. Wireless Commun.*, vol. 12, no. 7, pp. 3622–3636, Jul. 2013.
[9] Y. Zeng and R. Zhang, "Full-duplex wireless-powered relay with self-energy recycling," *IEEE Wireless Commun. Lett.*, vol. 4, no. 2, pp. 201–204, Apr. 2015.
[10] G. Zhu, C. Zhong, H. A. Suraweera, G. K. Karagiannidis, Z. Zhang, and T. A. Tsiftsis, "Wireless information and power transfer in relay systems with multiple antennas and interference," *IEEE Trans. Commun.*, vol. 63, no. 4, pp. 1400–1418, Apr. 2015.
[11] B. Kellogg *et al.*, "Passive Wi-Fi: Bringing low power to Wi-Fi transmissions," in *Proc. 13th USENIX Symp. Netw. Syst. Design Implementation*, Mar. 2016, pp. 151–164.
[12] V. Iyer, V. Talla, B. Kellogg, S. Gollakota, and J. Smith, "Inter-technology backscatter: Towards Internet connectivity for implanted devices," in *Proc. ACM SIGCOMM*, 2016, pp. 356–369.
[13] G. Yang and Y. C. Liang, "Backscatter communications over ambient OFDM signals: Transceiver design and performance analysis," in *Proc. IEEE GLOBECOM*, Dec. 2016, pp. 1–6.
[14] G. Wang, F. Gao, R. Fan, and C. Tellambura, "Ambient backscatter communication systems: Detection and performance analysis," *IEEE Trans. Commun.*, vol. 64, no. 11, pp. 4836–4846, Nov. 2016.
[15] D. Darsena, G. Gelli, and F. Verde, "Modeling and performance analysis of wireless networks with ambient backscatter devices," *IEEE Trans. Commun.*, vol. 65, no. 4, pp. 1797–1814, Jan. 2017.
[16] D. Arnitz and M. S. Reynolds, "Multitransmitter wireless power transfer optimization for backscatter RFID transponders," *IEEE Antennas Wireless Propag. Lett.*, vol. 12, pp. 849–852, 2013.
[17] G. Yang, C. K. Ho, and Y. L. Guan, "Multi-antenna wireless energy transfer for backscatter communication systems," *IEEE J. Sel. Areas Commun.*, vol. 33, no. 12, pp. 2974–2987, Dec. 2015.
[18] K. Han and K. Huang, "Wirelessly powered backscatter communication networks: Modeling, coverage, and capacity," *IEEE Trans. Wireless Commun.*, vol. 16, no. 4, pp. 2548–2561, Apr. 2017.
[19] D. T. Hoang, D. Niyato, P. Wang, D. I. Kim, and Z. Han, "Ambient backscatter: A new approach to improve network performance for RF-powered cognitive radio networks," *IEEE Trans. Commun.*, vol. 65, no. 9, pp. 3659–3674, Sep. 2017.

[20] D. T. Hoang, D. Niyato, P. Wang, D. I. Kim, and L. B. Le, "Optimal data scheduling and admission control for backscatter sensor networks," *IEEE Trans. Commun.*, vol. 65, no. 5, pp. 2062–2077, May 2017.
[21] S. Gong, L. Duan, and N. Gautam, "Optimal scheduling and beamforming in relay networks with energy harvesting constraints," *IEEE Trans. Wireless Commun.*, vol. 15, no. 2, pp. 1226–1238, Feb. 2016.
[22] Z. Ding, S. M. Perlaza, I. Esnaola, and H. V. Poor, "Power allocation strategies in energy harvesting wireless cooperative networks," *IEEE Trans. Wireless Commun.*, vol. 13, no. 2, pp. 846–860, Feb. 2014.
[23] J. Kimionis, A. Bletsas, and J. N. Sahalos, "Increased range bistatic scatter radio," *IEEE Trans. Commun.*, vol. 62, no. 3, pp. 1091–1104, Mar. 2014.
[24] C. He, "MIMO backscatter RFID systems: Performance analysis, design and comparison," Ph.D. dissertation, Dept. Elect. Comput. Eng., Univ. British Columbia, Vancouver, BC, Canada, 2014. [Online]. Available: https://open.library.ubc.ca/cIRcle/collections/24/items/1.0103398
[25] G. Yang, Y.-C. Liang, and Q. Zhang, "Cooperative receiver for ambient backscatter communications with multiple antennas," in *Proc. IEEE ICC*, Paris, France, May 2017, pp. 1–6.
[26] B. Lyu, Z. Yang, G. Gui, and Y. Feng, "Wireless powered communication networks assisted by backscatter communication," *IEEE Access*, vol. 5, pp. 7254–7262, 2017.
[27] R. Zhang and C. K. Ho, "MIMO broadcasting for simultaneous wireless information and power transfer," *IEEE Trans. Wireless Commun.*, vol. 12, no. 5, pp. 1989–2001, May 2013.
[28] S. J. Thomas, E. Wheeler, J. Teizer, and M. S. Reynolds, "Quadrature amplitude modulated backscatter in passive and semipassive UHF RFID systems," *IEEE Trans. Microw. Theory Techn.*, vol. 60, no. 4, pp. 1175–1182, Apr. 2012.
[29] G. De Vita and G. Iannaccone, "Design criteria for the RF section of UHF and microwave passive RFID transponders," *IEEE Trans. Microw. Theory Techn.*, vol. 53, no. 9, pp. 2978–2990, Sep. 2005.
[30] E. Boshkovska, D. W. K. Ng, N. Zlatanov, and R. Schober, "Practical non-linear energy harvesting model and resource allocation for SWIPT systems," *IEEE Commun. Lett.*, vol. 19, no. 12, pp. 2082–2085, Dec. 2015.
[31] Z.-Q. Luo, W.-K. Ma, A. M.-C. So, Y. Ye, and S. Zhang, "Semidefinite relaxation of quadratic optimization problems," *IEEE Signal Process. Mag.*, vol. 27, no. 3, pp. 20–34, May 2010.
[32] Y. Nesterov and A. Nemirovskii, *Interior-Point Polynomial Algorithms in Convex Programming*. Philadelphia, PA, USA: SIAM, 1994.
[33] A. A. Nasir, H. D. Tuan, T. Q. Duong, and H. V. Poor, "Secrecy rate beamforming for multicell networks with information and energy harvesting," *IEEE Trans. Signal Process.*, vol. 65, no. 3, pp. 677–689, Feb. 2017.
[34] A. A. Nasir, H. D. Tuan, T. Q. Duong, and H. V. Poor, "Secure and energy-efficient beamforming for simultaneous information and energy transfer," *IEEE Trans. Wireless Commun.*, vol. 16, no. 1, pp. 7523–7537, Nov. 2017.
[35] K. Huang and N. D. Sidiropoulos, "Consensus-ADMM for general quadratically constrained quadratic programming," *IEEE Trans. Signal Process.*, vol. 64, no. 20, pp. 5297–5310, Oct. 2016.
[36] Z. Xiang and M. Tao, "Robust beamforming for wireless information and power transmission," *IEEE Wireless Commun. Lett.*, vol. 1, no. 4, pp. 372–375, Aug. 2012.
[37] R. Zhang and Y.-C. Liang, "Exploiting multi-antennas for opportunistic spectrum sharing in cognitive radio networks," *IEEE J. Sel. Topics Signal Process.*, vol. 2, no. 1, pp. 88–102, Feb. 2008.
[38] I. Pölik and T. Terlaky, "A survey of the S-Lemma," *SIAM Rev.*, vol. 49, no. 3, pp. 371–418, 2007.
[39] S. X. Wu, X. Ni, and A. M.-C. So, "A polynomial optimization approach for the robust beamforming design in a device-to-device two-hop one-way relay network," in *Proc. IEEE ICASSP*, Mar. 2016, pp. 3841–3845.

Shimin Gong (M'15) received the B.E. and M.E. degrees in electrical engineering from the Huazhong University of Science and Technology, Wuhan, China, in 2008 and 2012, respectively, and the Ph.D. degree in computer engineering from Nanyang Technological University, Singapore, in 2014. He was a Visiting Scholar with The Chinese University of Hong Kong, Hong Kong, in 2011, and the University of Waterloo, Waterloo, ON, Canada, in 2012. He is currently an Associate Professor with the Shenzhen Institutes of Advanced Technology, Chinese Academy of Sciences. His research interests include wireless powered D2D networks, mobile edge computing, and backscatter communications and networking.

Xiaoxia Huang (M'07) received the B.E. and M.E. degrees in electrical engineering from the Huazhong University of Science and Technology, Wuhan, China, in 2000 and 2002, respectively, and the Ph.D. degree in electrical and computer engineering from the University of Florida, Gainesville, FL, USA, in 2007. She is currently a Professor with the College of Information Engineering, Shenzhen University, Shenzhen, China. Her research interests include cognitive radio networks, energy harvesting, smart phone applications, wireless sensor networks, and wireless communications.

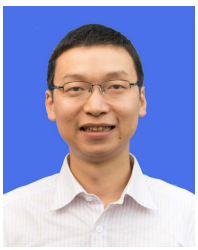

Jing Xu (M'15) received the B.S. degree in telecommunication engineering and the Ph.D. degree in electronics and information engineering from the Huazhong University of Science and Technology, Wuhan, China, in 2001 and 2011, respectively. He is currently an Associate Professor with the School of Electronic Information and Communications, Huazhong University of Science and Technology. His research interests include wireless networks and network security, with a special focus on performance optimization, game theory, and reinforcement learning and their application in networked systems.

Wei Liu (M'07) received the B.S. degree in telecommunication engineering and the Ph.D. degree in electronics and information engineering from the Huazhong University of Science and Technology, Wuhan, China, in 1999 and 2004, respectively. He is currently an Associate Professor with the School of Electronic Information and Communications, Huazhong University of Science and Technology. His research interests include wireless networks, Internet measurement, and content centric networks.

Ping Wang (M'08–SM'15) received the Ph.D. degree in electrical engineering from the University of Waterloo, Canada, in 2008. She is currently an Associate Professor with the School of Computer Science and Engineering, Nanyang Technological University, Singapore. Her current research interests include resource allocation in wireless networks, cloud computing, and smart grid. She was a co-recipient of the Best Paper Award from the IEEE International Conference on Communications in 2007 and the IEEE Wireless Communications and Networking Conference in 2012.

Dusit Niyato (M'09–F'17) received the B.Eng. degree from the King Mongkut's Institute of Technology Ladkrabang, Thailand, in 1999, and the Ph.D. degree in electrical and computer engineering from the University of Manitoba, Canada, in 2008. He is currently a Professor with the School of Computer Science and Engineering, Nanyang Technological University, Singapore. His research interests are in the area of energy harvesting for wireless communication, Internet of Things, and sensor networks.